

SHORT WAVE INFRARED CAMERA DESIGN AND FOCAL PLANE  
ANALYSIS

A THESIS SUBMITTED TO  
THE GRADUATE SCHOOL OF NATURAL AND APPLIED SCIENCES  
OF  
MIDDLE EAST TECHNICAL UNIVERSITY

BY

TUĞBA BOLAT BELDEK

IN PARTIAL FULFILLMENT OF THE REQUIREMENTS  
FOR  
THE DEGREE OF MASTER OF SCIENCE  
IN  
PHYSICS

FEBRUARY 2012

Approval of the thesis:

**SHORT WAVE INFRARED CAMERA DESIGN AND FOCAL PLANE  
ANALYSIS**

submitted by **TUĞBA BOLAT BELDEK** in partial fulfillment of the requirements for the degree of **Master of Science in Physics Department, Middle East Technical University** by,

Prof. Dr. Canan Özgen \_\_\_\_\_  
Dean, Graduate School of **Natural and Applied Sciences**

Prof. Dr. Mehmet T. Zeyrek \_\_\_\_\_  
Head of Department, **Physics**

Assoc. Prof. Dr. Akif Esendemir \_\_\_\_\_  
Supervisor **Physics Dept. METU**

**Examining Committee Members:**

Prof. Dr. İbrahim Günal \_\_\_\_\_  
Physics Dept., METU

Assoc. Prof. Dr. Akif Esendemir \_\_\_\_\_  
Physics Dept., METU

Assoc. Prof. Dr. Enver Bulur \_\_\_\_\_  
Physics Dept., METU

Asst. Prof. Dr. Sinan Kaan Yerli \_\_\_\_\_  
Physics Dept., METU

Dr. Ali Alaçakır \_\_\_\_\_  
TAEK

**Date:** \_\_\_\_\_ **10.02.2012**

**I hereby declare that all information in this document has been obtained and presented in accordance with academic rules and ethical conduct. I also declare that, as required by these rules and conduct, I have fully cited and referenced all material and results that are not original to this work.**

**Name, Last name:** Tuğba BOLAT BELDEK

**Signature** :

## **ABSTRACT**

### **SHORT WAVE INFRARED IMAGING SYSTEM DESIGN AND FOCAL PLANE ANALYSIS**

Bolat Beldek, Tuğba

M.Sc., Department of Physics

Supervisor: Assoc. Prof. Dr. Akif Esendemir

February 2012, 68 pages

The subject of this study is the design of a camera, which has maximum volume of 50 mm x 50 mm x 300 mm, using short infrared wavelength providing Rayleigh criteria. Firstly, the required flux per pixel has been calculated. Throughout these calculations, atmospheric losses have been obtained by MODTRAN program. Also signal to noise ratio has been examined at minimum and maximum integration time intervals. The focal length of the camera has been calculated as it receives 1 m resolution from 8 km distance. Moreover, the lens materials have been used as N-F<sub>2</sub>, LIF and BaF<sub>2</sub> in this six lens system. The design has been done using ZEMAX optical design program and the performance of the system at focal plane was investigated by the help of Seidel aberrations, Modulation transfer Function (MTF), Spot diagram and Optical Path Difference (OPD) fan plot analyses.

Keywords: SWIR, Optical design, Atmospheric transmission, ZEMAX

## ÖZ

### KISA KIZILÖTESİ DALGA BOYUNDA KAMERA TASARIMI VE ODAK DÜZLEMİ ANALİZLERİ

Bolat Beldek, Tuğba

Yüksek Lisans, Fizik Bölümü

Tez Yöneticisi: Doç. Dr. Akif Esendemir

Şubat 2012, 68 sayfa

Bu çalışmanın konusu kısa kızılötesi dalga boyunda Rayleigh kriterlerine uygun ve en fazla 50 x 50 x 300 mm boyutlarında kamera tasarımıdır. Öncelikle bir pixel için gerekli akı hesaplanmıştır. Akı hesabı yapılırken atmosferik kayıplar MODTRAN programında hesaplanmıştır. En kısa ve en uzun entegrasyon zaman aralıklarında sinyal gürültü oranına bakılmıştır. Kameranın odak uzaklığı 8 km uzaklıktan 1 m çözünürlüğünde görüntü alabilecek şekilde hesaplanmış ve altı mercekli kırıcı bir sistem kullanılarak tasarlanan sistemde cam cinsi olarak N-F<sub>2</sub>, LIF, BaF<sub>2</sub> kullanılmıştır. Tasarım, ZEMAX optik tasarım programı kullanılarak yapılmış ve Seidel aberasyonları, Modülasyon transfer fonksiyonu (MTF), spot diyagramı ve optik yol farkı gibi analizlerle tasarımın bu odak düzlemindeki performansı incelenmiştir.

Anahtar Kelimeler: SWIR, Optik tasarım, Atmosferik geçirgenlik, ZEMAX

## ACKNOWLEDGEMENTS

First of all, I would like to thank my supervisor Assoc. Prof. Dr. Akif ESENDEMİR for his kind guidance, cooperation, encouragement and advice throughout the study.

I would like to thank Prof. Dr. İbrahim GÜNAL for his discussions and encouragement.

I sincerely thank ROKETSAN and the managers for giving me the chance to complete my Master of Science degree.

I express my deepest gratitude to my mother Emine BOLAT for her endless love, moral, and encouragement.

Also, I would like to thank my darling Arif BELDEK for his existence, trust, endurance.

And finally to my daughter...

## TABLE OF CONTENTS

ABSTRACT .....	iv
ÖZ.....	v
ACKNOWLEDGEMENTS .....	vi
TABLE OF CONTENTS .....	vii
LIST OF FIGURES.....	ix
LIST OF TABLES .....	xi
CHAPTERS.....	xi
1 INTRODUCTION.....	1
2 BACKGROUND INFORMATION.....	4
2.1 Electromagnetic Spectrum.....	4
2.1.1 SWIR .....	5
2.2 Atmosphere.....	7
2.2.1 Atmospheric Transmission.....	9
2.2.2 MODTRAN.....	11
2.3 Optical Design .....	11
2.3.1 Seidel Aberrations .....	12
2.3.2 Rayleigh Quarter Wave Limit .....	18
2.3.3 Zemax.....	23
3 SYSTEM DESIGN.....	28
3.1 System Requirements .....	28
3.1.1 Focal Length and f- number .....	29
3.1.2 Flux Calculation .....	31
3.1.3 Signal to Noise Ratio Calculation .....	38
3.1.4 Rayleigh Resolution Criteria .....	40

3.2	Optical Design .....	41
3.2.1	Glass Selection .....	45
3.3	System Performance .....	47
3.3.1	Seidel Aberrations .....	47
3.3.1.1	Distortion .....	49
3.3.1.2	Field Curvature .....	50
3.3.1.3	Lateral Color .....	51
3.3.1.4	Chromatic Focal Shift .....	52
3.3.2	Spot Diagram.....	53
3.3.3	Enclosed Energy.....	56
3.3.4	MTF.....	57
3.3.5	Vignetting.....	58
4	DISCUSSION AND CONCLUSION .....	61
	REFERENCES.....	65

## LIST OF FIGURES

### FIGURES

Figure 2-1. Electromagnetic Spectrum [1] .....	4
Figure 2-2. SWIR and thermally uniform scenes [3] .....	6
Figure 2-3. Day time images of forest fire [4] .....	6
Figure 2-4. Structure of the atmosphere [7] .....	8
Figure 2-5. Atmospheric windows [11] .....	10
Figure 2-6. Basic ray trace .....	11
Figure 2-7. Spherical aberration.....	14
Figure 2-8. Chromatic aberration .....	14
Figure 2-9. Coma.....	15
Figure 2-10. Astigmatism.....	16
Figure 2-11. Field curvature .....	17
Figure 2-12. Distortion .....	17
Figure 2-13. OPD [18].....	19
Figure 2-14. OPD [18].....	20
Figure 2-15. OPD vs. Y [18] .....	22
Figure 2-16. Spot Diagram settings tool .....	24
Figure 2-17. Spot Diagram.....	25
Figure 2-18. Spot diagrams and their ray fan plots .....	26
Figure 2-19. MTF vs. frequency .....	27
Figure 3-1 Relation between $f_{\text{eff}}$ , resolution, pixel size and distance of the camera from ground.....	29
Figure 3-2. ASTM G-173-03 Reference spectra for solar irradiance [26] .....	32
Figure 3-3. Wavelength vs. radiation before entering the ground.....	33

Figure 3-4. Wavelength vs. reflection coefficient for green grass [7] .....	33
Figure 3-5. Wavelength vs. radiation after reflection from ground .....	34
Figure 3-6. Transmission of atmosphere .....	35
Figure 3-7. Transmission ratio for 8 km distance .....	36
Figure 3-8. Wavelength vs. irradiation on the detector .....	36
Figure 3-9 Wavelength vs. total photon number on the detector .....	37
Figure 3-10. Wavelength vs. electrons on the detector. ....	38
Figure 3-11. Integration time vs. S/N.....	39
Figure 3-12. Radius of the airy disk vs. wavelength .....	40
Figure 3-13. 2D layout of designed system.....	44
Figure 3-14. Internal transmission graph for the N-F <sub>2</sub> , lenses through 10 mm thickness .....	45
Figure 3-15. Internal transmission graph for the LiF lenses .....	46
Figure 3-16. Internal transmission graph for the BaF <sub>2</sub> lenses .....	46
Figure 3-17. Primary aberrations for each surface and sum of them on the image plane .....	48
Figure 3-18. OPD fan plot for 3 fields .....	49
Figure 3-19. Grid distortion for 5 degree field.....	50
Figure 3-20 Field curvature .....	51
Figure 3-21. Lateral color.....	52
Figure 3-22. Choromatic focal shift .....	53
Figure 3-23. Spot diagram for different fields. ....	54
Figure 3-24. Spot diagram after shifting the focus 30 μm. ....	55
Figure 3-25. Spot diagram after shifting the focus 50 μm .....	55
Figure 3-26. Fraction of enclosed energy.....	56
Figure 3-27. MTF .....	58
Figure 3-28. Vignetting diagram .....	59
Figure 3-29. Vignetting diagram after optimization. ....	59

## LIST OF TABLES

### TABLES

Table 1. Detector parameters [23],[24],[25].....	29
Table 2. System prescription data .....	43
Table 3 System lens parameters .....	44
Table 4. Numerical values of Seidel aberrations (in $\lambda$ ). .....	47
Table 5. Numerical values of transmission .....	60
Table 6. Parameters of the lenses and result of analysis after test plate optimization .....	63

## **CHAPTER 1**

### **INTRODUCTION**

The objective of this study is to calculate the flux and design a camera system to take image in the SWIR (Short wave Infrared )range. Since visible range is limited in bad weather conditions for imaging and thermal range is limited with temperature difference, SWIR cameras have advantage and provide superior imaging to see the objects through haze, fog, smoke, dust and without temperature dependence as compared to visible and thermal imagers. Most popular imaging sensors are Indium Gallium Arsenide (InGaAs) sensors.

Atmospheric transmittance is limited by atmospheric conditions, and is a function of wavelength. As a result, the change in atmospheric transmittance is not the same for all the wavelengths. So, the performance of the electro-optical systems depends on the used wavelength. In order to obtain the sufficient flux, these atmospheric effects are taken into consideration and MODTRAN (MODERATE RESOLUTION TRANSMITTANCE CODE) is utilized for the necessary calculations.

The camera was designed to take images from 8 km distance and 4-5 km height from the ground, 1 m resolution and  $10^\circ$  field of view which corresponds to the 1400 x 1400 m sweep area. There is also space requirement which is 50 x 50 x 300 mm to install the camera system. The system is designed as a refractive system. In

order to obtain good performance, Rayleigh criteria are taken into account and used to achieve an aberration free and diffraction limited system. And also to obtain this performance, six lenses are used and the glasses are selected as N-F<sub>2</sub>, LIF, BaF<sub>2</sub> because of their high transmission values in the Short Wave Infrared (SWIR) range.

The designed camera system has also ability to take images in the visible region depending on the type of the imaging detector used.

The relation between the pixel size and the resolution has been determined for main wavelengths. To obtain best performance at the focal surface, the ZEMAX program is used to simulate the parameters like radius of curvature, thickness, and the position of the lenses. The simulations are repeated many times for the different field angles. In addition to these simulations, to evaluate the performances of the designed optics, the performance tests like aberrations, spot diagram, MTF, vignetting, and distortion have been carried out. Furthermore, the necessary calculations have been done to determine the properties like focal length, F#number, detector size, and swept area. The designed camera has been optimized by using the merit function and analyzed with the focal plane simulations.

In the following chapters, the details of the study are presented.

In Chapter 2, an overview of the literature of atmospheric transmission and atmospheric effects and their influence on optical transmission are introduced. Basic definitions and some brief information about analysis tools like Zemax and Modtran are also given.

In Chapter 3 flux and Signal to Noise ratio (S/N) calculations are carried out. Their outputs are plotted, which is necessary for determining one of the pixels efficiency calculations. Moreover design and optimization of the system for best performance have been done. Results are described, plotted and discussed.

In Chapter 4 finally, the study is concluded briefly indicating the significant parts.

## CHAPTER 2

### BACKGROUND INFORMATION

#### 2.1 Electromagnetic Spectrum

The interaction of light with solids, particles and gasses is sensitive to wavelength. As a consequence, the relationship between intensity and wavelength generally carries much of the information about the objects which the radiation has touched. As seen in Figure 2-1, different length units are used in order to describe the magnitude of wavelength, since this spectrum is big the most commonly used are micron and nanometer for very short wavelengths, millimeter, centimeter or meter for longer ones. Also the electromagnetic radiation spectrum is divided into following categories; which are their usage area, gamma rays, X-rays, ultraviolet, visible, infrared, microwave and radio waves. These categories also divided into sub-categories like SWIR, MWIR (Midwave Infrared) and LWIR (Longwave Infrared) for infrared region.

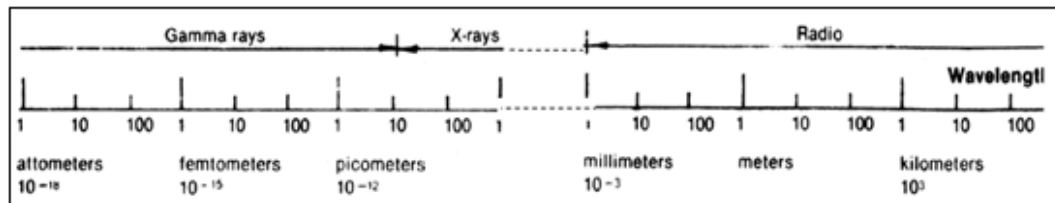


Figure 2-1. Electromagnetic Spectrum [1]

There are many sources for radiation but the Sun is one of the most interesting sources of light because of its dynamic output. Thus scientists have been fascinated with the sun and the behavior of its electromagnetic radiation output for ages. [2]

### **2.1.1 SWIR**

Development of InGaAs (Indium Gallium Arsenide) sensors makes it possible to sense the SWIR part of the electromagnetic spectrum which extends from 0.9 to 1.7 microns. SWIR light connects the spectral gap between visible and thermal bands.

Wavelengths longer than visible wavelengths can be detected by specialized sensors and the most popular sensors for SWIR are InGaAs sensors. Although light in the SWIR range is not visible to the human eye, this light interacts with objects in a similar manner as visible wavelengths. And the image occurs with the reflected light as in the visible range.

Sensors which operate in the MWIR and LWIR range detect thermal emissions from the objects. If there is no a temperature difference between the object of interest and the surrounding environment, it is impossible to detect the object. Also MWIR and LWIR sensors are characteristically not able to see significant details if there is not enough temperature difference. As seen in Figure 2-2, MWIR sensors fail to show any recognizable detail of the object because of lack of temperature difference.

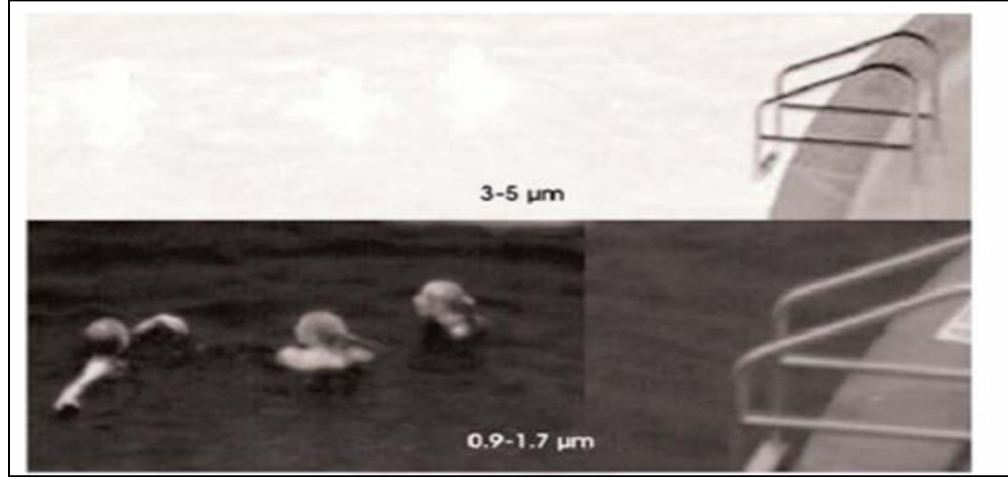


Figure 2-2. SWIR and thermally uniform scenes [3]

SWIR allows seeing greater details of objects and recognizing targets like visible light since in this range reflected light is used to form the image like visible imaging sensors. In addition to this advantage, due to the reduced Rayleigh scatter of light at longer wavelengths, IR light can travel easily through haze, fog, dust and high humidity, so SWIR cameras can see better through these conditions than visible cameras. As seen in Figure 2-3, the fire seems to be seen clearer with the SWIR than visible light.



Figure 2-3. Day time images of forest fire [4]

Thus, development of SWIR sensors and cameras overcomes these problems and started to use different fields from medical to military applications [5].

## **2.2 Atmosphere**

The atmosphere surrounds and protects the earth and it acts as a shield against harmful radiation and meteors. During the propagation throughout it, the electromagnetic spectrum suffers from some degree of from absorption of the electromagnetic energy by the atmospheric gases and from attenuation by atmospheric aerosols [6]. Optical propagation in this medium has many important characteristics and consequences for remote sensing, electro-optical system performance etc.

As seen in Figure 2-4, the atmosphere is composed of gases and suspended particles at various temperatures and pressures as a function of altitude and azimuth. It is composed of six main horizontal layers starting from troposphere, stratosphere, mesosphere, ionosphere, thermosphere and at the upper layer exosphere.

Most of the important atmospheric attenuators ( $H_2O$ ,  $CO_2$ , clouds, fogs, aerosols, etc.) exist in the first layer, which extends from ground to approximately 11 km altitude. As seen in Figure 2-4, in this layer, pressure and density are highest and so the highest molecular scattering occurs. [7]

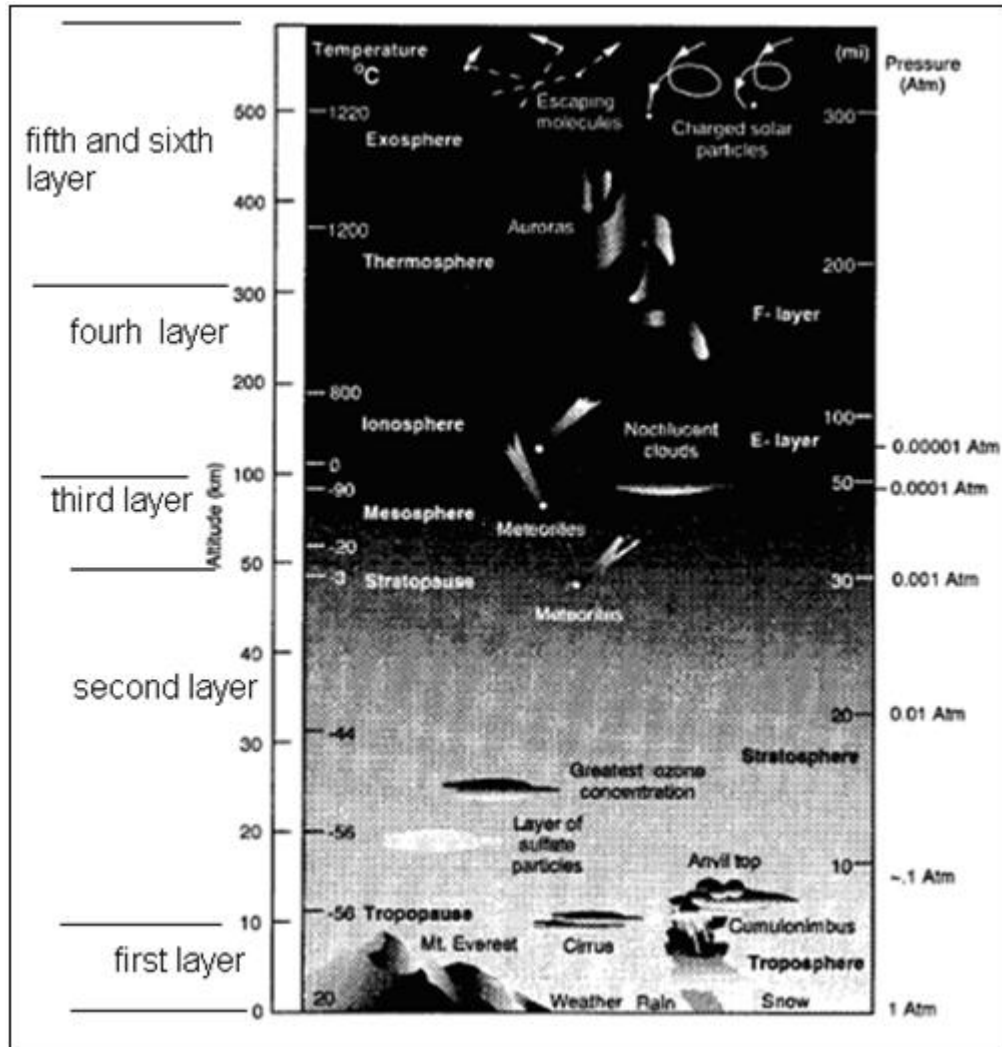


Figure 2-4. Structure of the atmosphere [7]

The second layer extends to the 50 km altitude from the ground and contains ozone which absorbs the ultraviolet radiation. The third layer extends to the 90 km altitude and most of the models concerning optical propagation end with this layer. The fourth layer is important for radio-wave propagation and extends to the 300 km altitude; the fifth and sixth layers are influenced by the solar radiation and extend to the 500 km altitude.

### 2.2.1 Atmospheric Transmission

The solar radiation passes through the atmosphere before reaching the entrance aperture of an optical system. As stated before, Earth's atmosphere is a mixture of various gases with varying characteristics of absorption, emission, and scattering of radiation.

The first phenomenon is molecular absorption. Water vapor, carbon dioxide, ozone, and some other molecules cause the molecular absorption. The second one is aerosol absorption. Particles like dust, ash and etc., cause the aerosol absorption in the atmosphere. The third one is aerosol scattering. If the wavelength is approximately the same size with the particle diameter, it causes the aerosol scattering called as Mie scattering and it is proportional to  $1/\lambda^2$ . And other important scattering phenomenon is molecular scattering and called Rayleigh scattering. Rayleigh scattering can be utilized to calculate the scattering due to the particles which are much smaller compared to the wavelength of incident electromagnetic wave. Rayleigh scattering occurs when particles are far less than a wavelength in diameter ( $\sim 0.03 \mu\text{m}$  diameter) and it is proportional to  $1/\lambda^4$  [8] [9].

Absorption and scattering are grouped together and called as extinction. This causes the reduction in the flux of the radiation through the atmosphere and expressed in terms of an exponential coefficient, in Beer's law;

$$\tau = e^{-\mu R} \quad (2.1)$$

Where;

$\tau$ = transmittance of a path length R through the atmosphere

$\mu$ = extinction coefficient

The total extinction coefficient is the sum of the coefficients of the total absorption and the total scattering. These coefficients depend on the density and molecular

composition of the atmosphere and number of density, compositions and the size distributions of the aerosols [10].

As a result of the atmospheric effects, the earth's atmosphere is opaque to large portions of the electromagnetic spectrum. Radiation reaching the observer in these wavelengths is absorbed and re-emitted by the atmosphere and does not contain information about the object which is tried to be observed. Whereas, as seen in Figure 2-5, there are several discrete portions of the spectrum for which the atmosphere is transparent. These spectral segments, which are known as "atmospheric windows" or just "windows", are defined by molecular absorption of primarily water vapor and carbon dioxide.

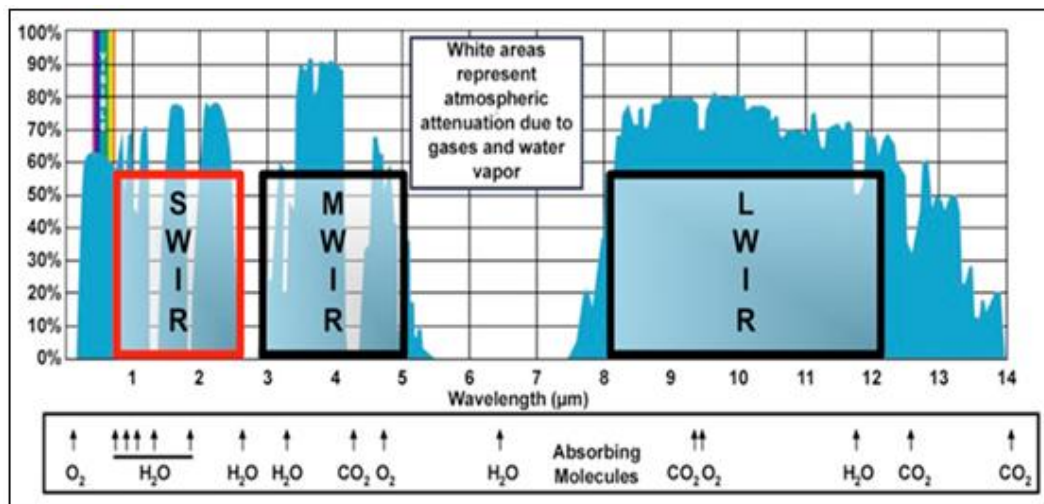


Figure 2-5. Atmospheric windows [11]

Some of these windows are;

- The visible/NIR window (0.4 to about 1.0 micron),
- The IR window (in the thermal IR between 8.0 and 12.0 microns)
- The microwave/radio window (wavelengths longer than about 1 cm.).

These windows are used in various electro optical systems together with matching sensors.

### 2.2.2 MODTRAN

MODTRAN is one of the popular computer codes for calculating atmospheric transmittance and radiance through complex mathematical algorithms and it has been developed over the past 30 years. It uses the HITRAN data base which defines atmosphere as parallel planes, sliced into 33 layers from 0 to 100 km altitude which have different physical parameters such as pressure, temperature, molecular absorption rate and extinction coefficients at each layer [12].

### 2.3 Optical Design

Before starting an optical design some optical concepts should be well understood to evaluate it. These concepts can be summarized as in Figure 2-6;

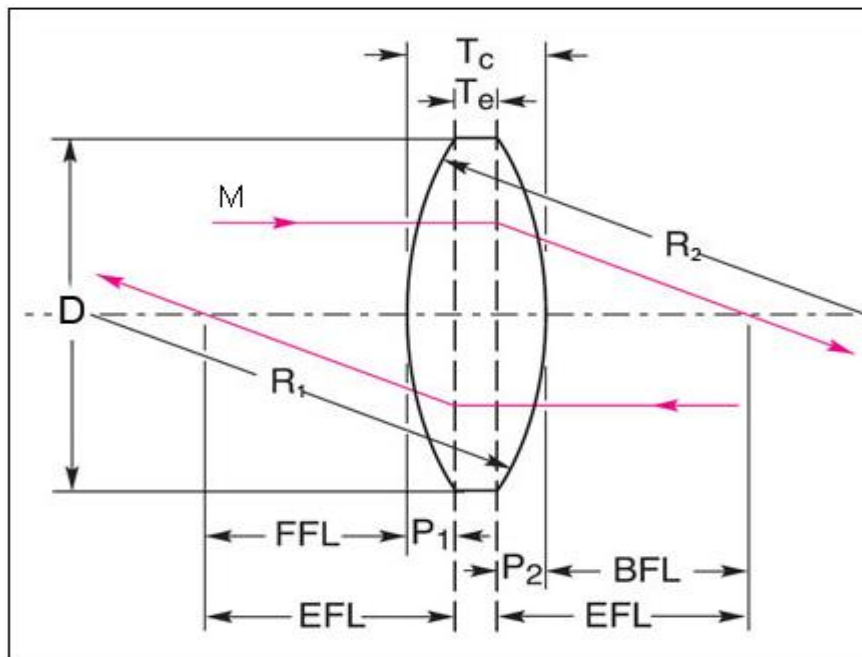


Figure 2-6. Basic ray trace

- EFL (Effective focal length) is the distance from the rear principal plane to the paraxial image surface.
- BFL (Back focal length) is the distance along the Z axis from the last surface made of glass to the paraxial image surface for the object at infinite conjugates.
- $T_e$  is the edge thickness of the lens
- $T_c$  is the central thickness of the lens
- D is the diameter of the lens
- Chief Ray is defined to be the ray that travels from a specific field point, through the center of the entrance pupil, and on to the image surface.
- The Marginal Ray is the ray that travels from the center of the object, to the edge of the entrance pupil, and on to the image surface.
- $P_1$  and  $P_2$  are the principal points
- FOV (Field of view) is the angular space from which the system accepts light [13].

### 2.3.1 Seidel Aberrations

Seidel published the first complete mathematical treatment of geometrical imagery which is called Seidel aberrations in 1856. These aberrations are spherical aberration, coma, astigmatism, field curvature, distortion. In addition to these ones there are also two main aberrations which are longitudinal and lateral chromatic aberration [14].

In order to determine image point Snell's law can be used at each optical surface to trace the path of light rays. When ray tracing is done, it is seen that not all the rays pass through the ideal point as in paraxial theory and these deviations from ideal imaging are known as lens aberrations. Their mathematical representations are given in Eq. 2.2.

$$W = W_{020}r^2 + W_{111}hr \cos \theta + W_{040}r^4 + W_{131}hr^3 \cos \theta + W_{222}hr^2 (\cos \theta)^2 + W_{220}h^2r^2 + W_{311}h^3r \cos \theta + \dots \quad (2.2)$$

Where;

W is the wavefront error function

h is height of the object

r and  $\theta$  are polar coordinates of the system aperture

$W_{020}$  Axial chromatic aberration

$W_{111}$  Tangential chromatic aberration

$W_{040}$  Spherical aberration

$W_{131}$  Coma

$W_{222}$  Astigmatism

$W_{220}$  Field curvature

$W_{311}$  Distortion

Starting from the Eq. 2.2, one can introduce the optical aberrations as follows.

- Spherical Aberration

Light rays striking the entrance aperture at different heights, but parallel to the optical axis as seen in Figure 2-7, this aberration is defined as variation of focus with aperture and it is directly related to the term  $r^4$  in Eq. 2.2 [15].

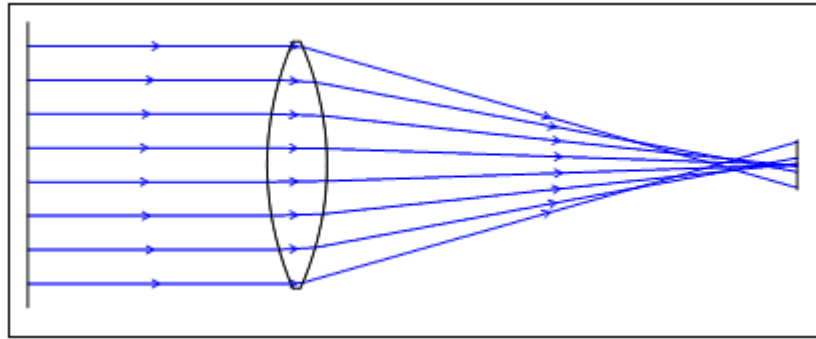


Figure 2-7. Spherical aberration

- Chromatic Aberration

Since index of refraction is a function of the wavelength, focal length differs with wavelength in the case of axial (longitudinal) chromatic aberration. On the other hand, in the transverse (lateral) aberration, magnification changes with wavelength. This type of aberration can be seen in Figure 2-8.

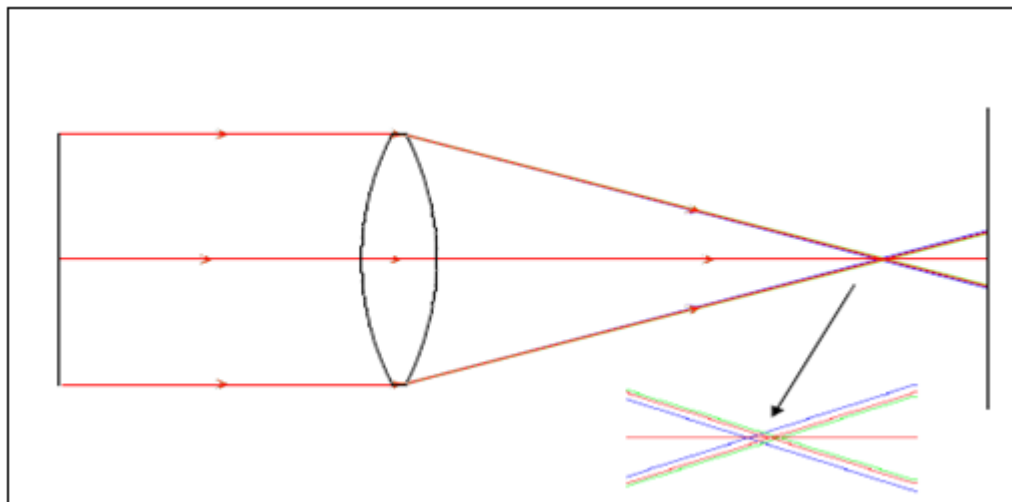


Figure 2-8. Chromatic aberration

As seen from Eq. 2.2 axial chromatic aberration value varies with  $r^2$  and transverse chromatic aberration varies with  $h$  and  $r$  terms.

- Coma

As seen in Figure 2-9, the effective focal lengths and transverse magnifications differ for rays coming from the off axis regions of the lens.

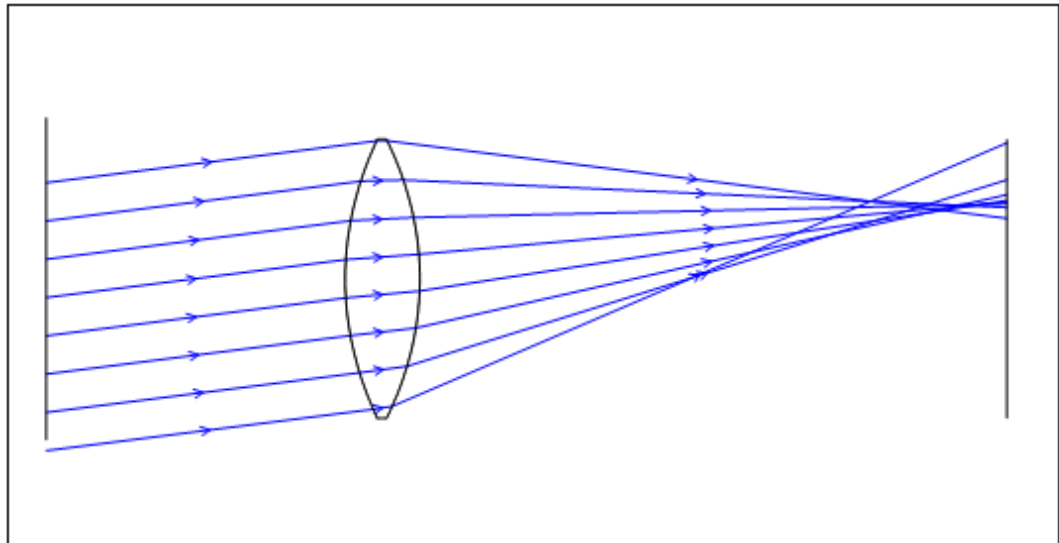


Figure 2-9. Coma

- Astigmatism

Off-axis rays on the meridional plane and sagittal plane form an image at different distances, as seen in Figure 2-10, thus a lens with astigmatism has two focal surfaces.

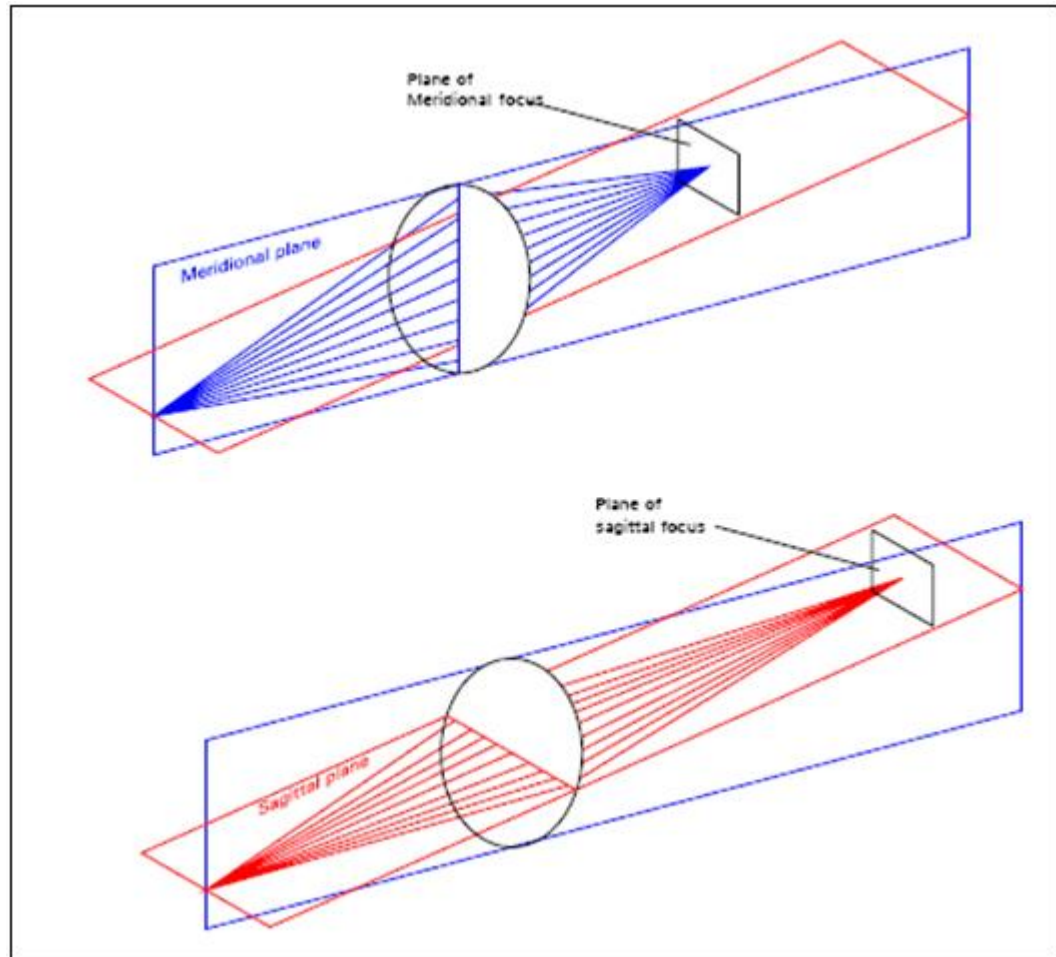


Figure 2-10. Astigmatism

- Field curvature

The image is formed on a curved surface. As seen in Figure 2-11 the reason for field curvature is usually a field-dependent defocus since back focal length changes with field zone.

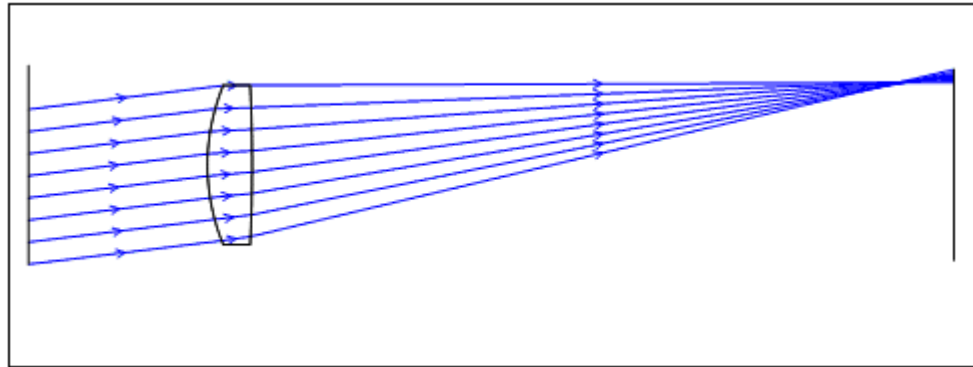


Figure 2-11. Field curvature

- Distortion

Distortion is a change in magnification as a function of field of view. So it defines the location of the images and has no effects on the sharpness or blurry of the images.

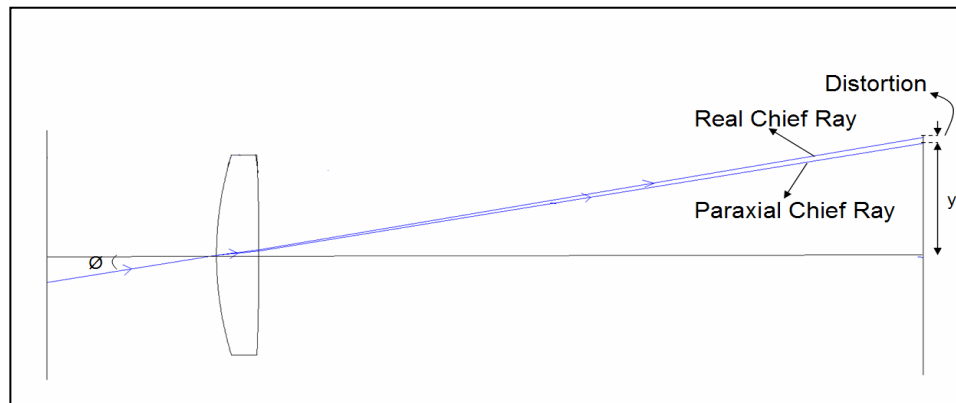


Figure 2-12. Distortion

As seen in Figure 2-12, magnification changes with  $\theta$ . If magnification is higher than the real chief ray height, it is called positive or pincushion distortion, if it is lower; it is called negative (barrel) distortion.

### **2.3.2 Rayleigh Quarter Wave Limit**

Ray tracing through the optical system gives chance to see wavefront deformation. In 1980, the optical path traveled by light rays through the optical system is directly obtained by doing ray tracing. According to Fermat's principle, the optical path of light rays from the point object to the image point is a constant if the image is perfect. However refracted wavefront does not have a perfect spherical shape and has some deformations due to fact that not all rays go to the ideal point image [16]. Thus, it is impossible to get perfect image quality, but it would be highly qualitative if the image of a point object could be formed as a perfect as possible [17]. And then the highest possible theoretical resolution can be obtained using an image-forming lens with small aberrations. According to the Rayleigh criterion, an optical system produces a diffraction-limited image if the peak to valley (PV) value of the wave front deformation has a maximum absolute value less than  $1/4$ .

Using the ray trace, the amount of the aberrations that corresponds a maximum wavefront error (one quarter-wave) is found. There are some different methods and basic one is the ray tracing.

- Out of focus,

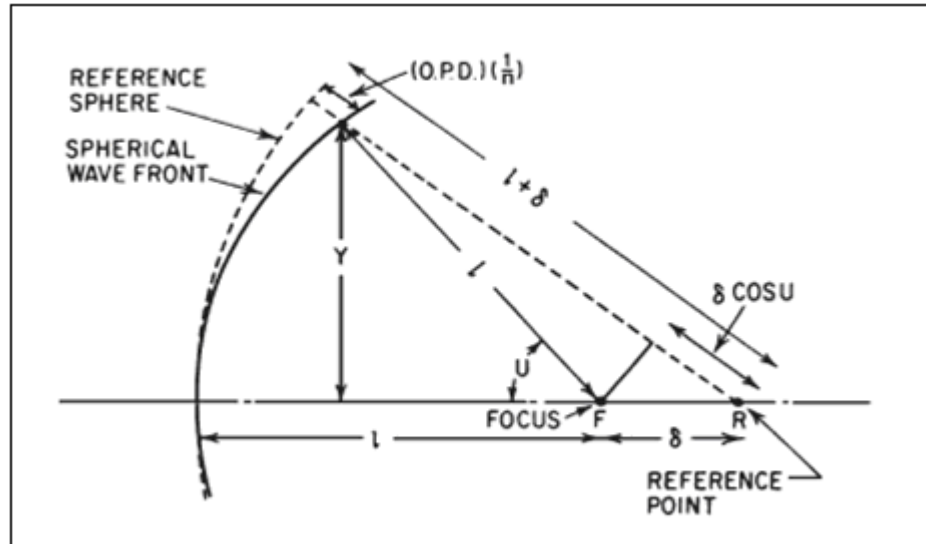


Figure 2-13. OPD [18]

From the Figure 2-13,

$$\frac{\text{OPD}}{n} = (1 + \delta - \delta \cos U - l) \quad (2.3)$$

Where;

OPD is wavefront error,

$\delta$  is the longitudinal shift from the reference sphere,

$U$  is the slope of the ray through the system,

$n$  is the index of the final medium

$l$  is the radius of the wavefront

$l + \delta$  is the radius of the reference sphere.

$$\frac{\text{OPD}}{n} = \delta(1 - \cos U) \quad (2.4)$$

Inserting the approximation,  $\cos U = (1 - \frac{1}{2} \sin^2 U)$  in the Eq. 2.4,

$$\text{OPD} = \frac{1}{2} n \delta \sin^2 U$$

from Rayleigh limit, for maximum aberration OPD is taken  $\lambda/4$ .

$$\frac{\lambda}{4} = \frac{1}{2} n \delta \sin^2 U \quad (2.5)$$

Focus shift is found,

$$\delta = \frac{\pm \lambda}{2n \sin^2 U_m} \text{ in longitudinal} \quad (2.6)$$

$U_m$  is the final slope of the marginal ray through the system.  $U_m$  is used because the maximum amount of OPD occurs at the edge of the wavefront.

- Spherical Aberration

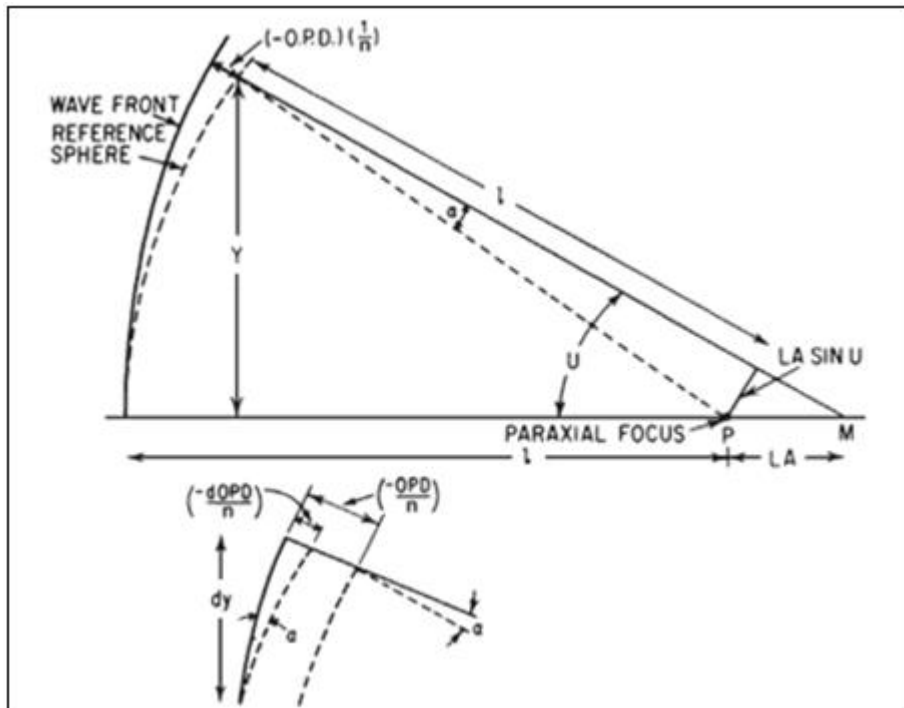


Figure 2-14. OPD [18]

From Figure 2-14,

$$\alpha = \frac{(-dOPD)}{ndY} \quad (2.7)$$

Also

$$\alpha = \frac{(LA) \sin U}{l} = \frac{(LA)Y}{l^2} \quad \text{and then} \quad (2.8)$$

$$\frac{(-dOPD)}{ndY} = \frac{(LA)Y}{l^2} \quad (2.9)$$

$$dOPD = \frac{-Yn(LA)dY}{l^2} \quad (2.10)$$

Longitudinal spherical aberration is a function of Y and its function known as  $LA=\sigma Y^2$  For third order spherical aberration, inserting this equation in the Eq. 2.10 and integrating it one obtains

$$OPD = -\int_0^Y \frac{nY}{l^2} (\sigma Y^2) dY \quad (2.11)$$

$$OPD = -\frac{n}{l^2} \left( \sigma \frac{Y^4}{4} \right) \Big|_0^Y \quad (2.12)$$

$$OPD = -\frac{nY^2}{2l^2} \left( \sigma \frac{Y^2}{2} \right) \quad (2.13)$$

where  $\sin U=Y/l$ , the Eq. 2.12 becomes;

$$OPD = -\frac{n \sin^2 U}{2} \left( \sigma \frac{Y^2}{2} \right) \quad (2.14)$$

Eq. 2.13 is the OPD with respect to the paraxial focus of the system.

$$OPD = \frac{n \sin^2 U}{2} \left( \delta - \sigma \frac{Y^2}{2} \right) \quad (2.15)$$

$$LA=\sigma Y^2$$

At the edge of the aperture  $Y=Y_m$  and  $LA=LA_m$ , putting these values into the Eq. 2.14, it reduces to;

$$\text{OPD} = \frac{n \sin^2 U}{2} \left( \delta - \frac{1}{2} LA_m \left( \frac{Y}{Y_m} \right)^2 \right)^2 \quad (2.16)$$

To find the smallest value of OPD for different values of  $\delta$ , some values were substituted, and OPD was plotted for each value as a function of  $Y$ .

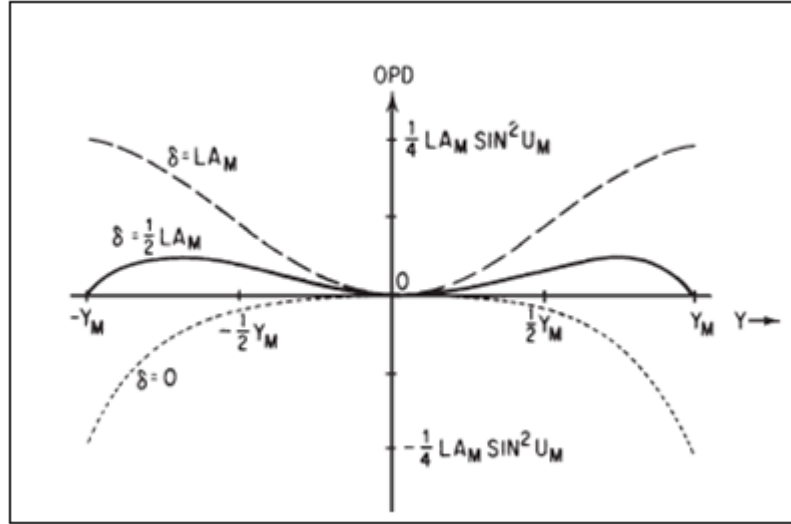


Figure 2-15. OPD vs.  $Y$  [18]

These values for  $\delta=0, 1/2(LA_m)$ ,  $LA_m$  as seen from the figure minimum value occurs at a point for  $\delta=1/2(LA_m)$ . This point is the best focus midway between the marginal and paraxial focal points. Putting the value  $\delta=1/2(LA_m)$  in the equation and differentiating it for maximum OPD with respect to  $Y$ .

$$\text{OPD} = \frac{n \sin^2 U}{2} \left( LA_m \frac{1}{2} - \frac{1}{2} LA_m \left( \frac{Y}{Y_m} \right)^2 \right)^2 \quad (2.17)$$

Sine is a function of  $Y$ , and putting  $\sin U = Y/l$  into Eq. 2.16, one can obtain;

$$d\text{OPD} = \left( \frac{n}{2l^2} \left( Y^2 LA_m \frac{1}{2} - \frac{1}{2} LA_m \frac{Y^4}{Y_m^2} \right) \right) dY \quad (2.18)$$

$$0 = 2Y - \frac{4Y^3}{Y_m^2} \quad (2.19)$$

$$Y = \sqrt{0,5} Y = 0,707 Y_m \quad (2.20)$$

Then,

$$OPD = \frac{LA_m}{16} n \sin^2 U_m \quad (2.21)$$

For one quarter wave OPD, marginal spherical aberration  $LA_m$  is found.

$$LA_m = \frac{\pm 4\lambda}{n \sin^2 U_m} \quad (2.22)$$

- Chromatic aberration

Longitudinal color is derived from the out of focus allowance; if the reference point is midway between the short and long wavelength focal points, it is apparent that they may be separated by twice the out of focus allowance before the Rayleigh limit is exceeded.

Then

$$L_{Ach} = L'_F - L'_C = \frac{\lambda}{n \sin^2 U_m} \quad (2.23)$$

### 2.3.3 Zemax

ZEMAX is a program which can model, analyze, and assist in the design of optical systems. This program uses ray tracing to model refractive, reflective and diffractive optics in a sequential and non-sequential mode. However, in order to use this program, program properly, one should have knowledge of an optical design, terminology and fundamentals of optics [19].

Some important analyze tools for ZEMAX can be summarized as follows;

- Spot Diagram

Spot diagram is the ray density at the focal plane and it gives a visual representation of the energy distribution in the image of a point object. To use this

tool, designer should state the necessary parameters like wavelength, field and the surface where the spot is formed. These can be done in settings tool shown in Figure 2-16;

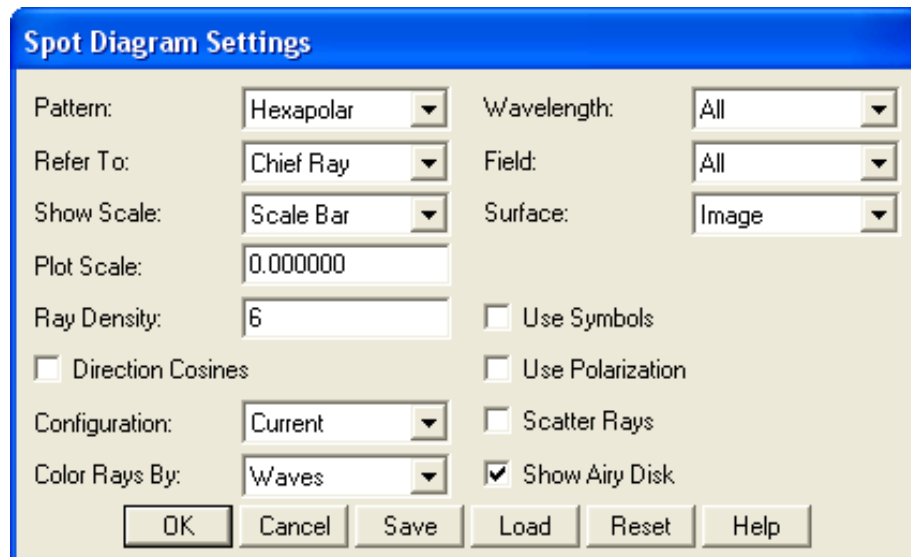


Figure 2-16. Spot Diagram settings tool

Spot diagram is useful for defining the some aberrations quickly as seen from the Figure 2-17. In this figure each spot diagram shows the deformation of the image of a point source in the case of different aberrations For example, in case of coma it is clear that spot has a comet like shape whereas in astigmatism elliptic spot is formed. Therefore, as it is stated before, spot diagram gives some idea about the system performance at first sight.

Another important point is the size of the spot. It is measure is called “Airy Disk” and defined as the first dark ring in the diffraction pattern. And its dimension can be calculated by using the Eq. 2.24.

$$\text{Airydisk } (\Gamma) = 1,22 \times \lambda \times f - \text{number} \quad (2.24)$$

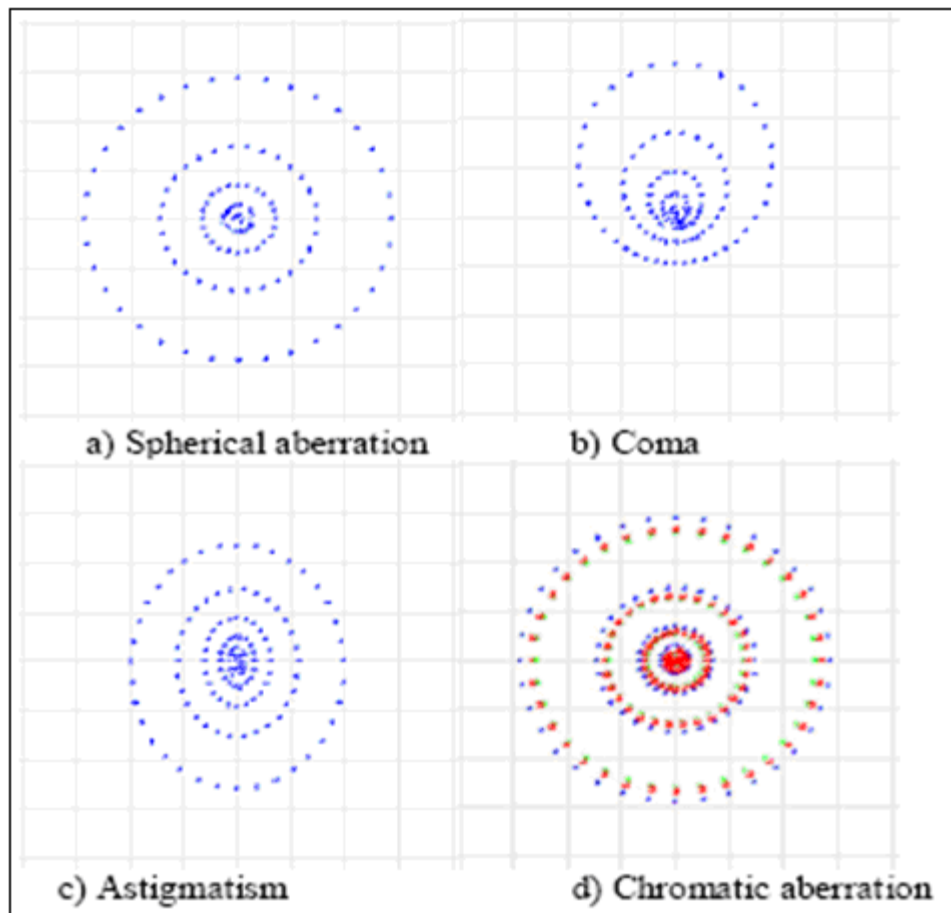


Figure 2-17. Spot Diagram

- Ray Fan

Ray fan is another way to see the aberrations in designed system through the aperture [20]. Except from the spot diagram, one can evaluate the aberrations through the pupil. In Figure 2-18, ray fan plot is plotted for different aberrations. In this figure, in order to see the difference between the aberrations, other aberrations are minimized and the defined aberration is tried to dominate.

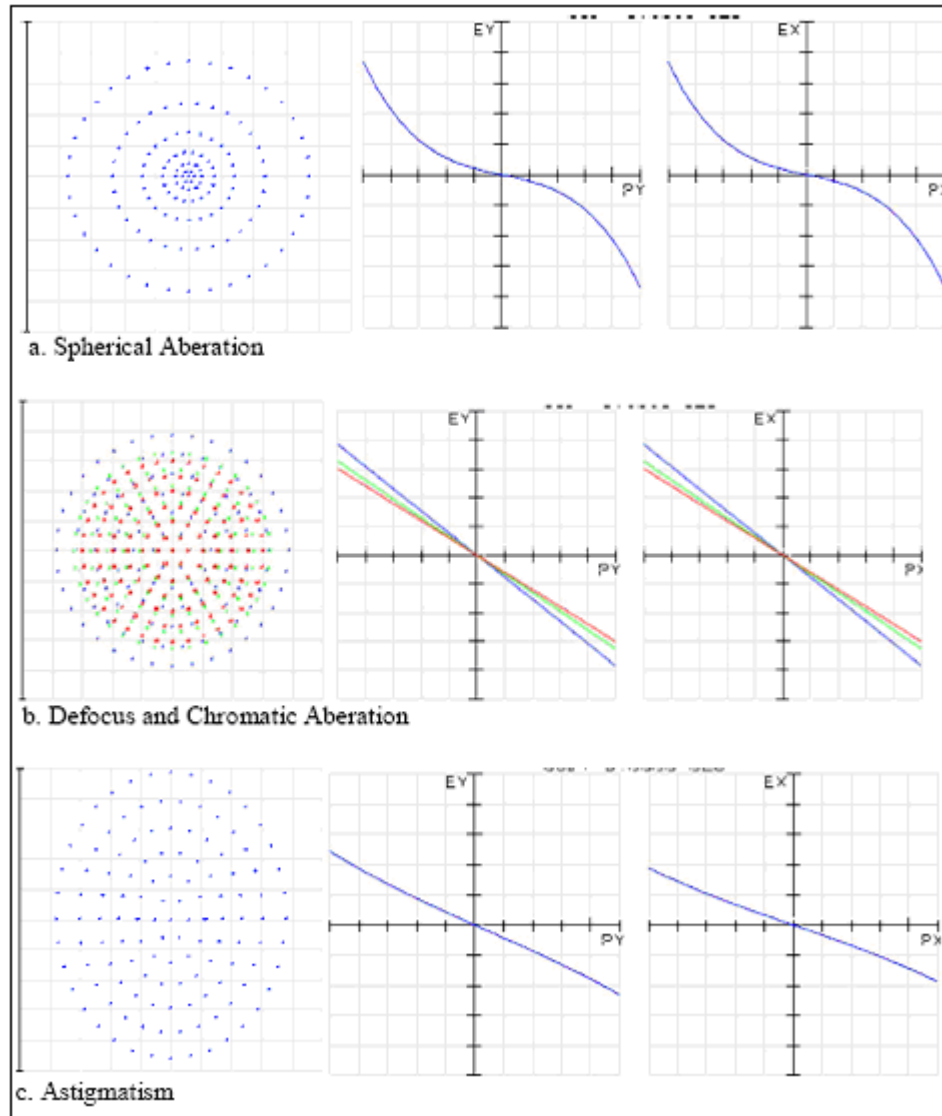


Figure 2-18. Spot diagrams and their ray fan plots

- MTF

MTF (modulation transfer function) is the main parameter used for system design, analysis and it describes the imaging resolution of the sensor. As seen in Figure 2-19, it is the output modulation produced by the system divided by the input

modulation at that spatial frequency [21]. At the cut off frequency, image modulation becomes nearly zero relative to the object modulation.

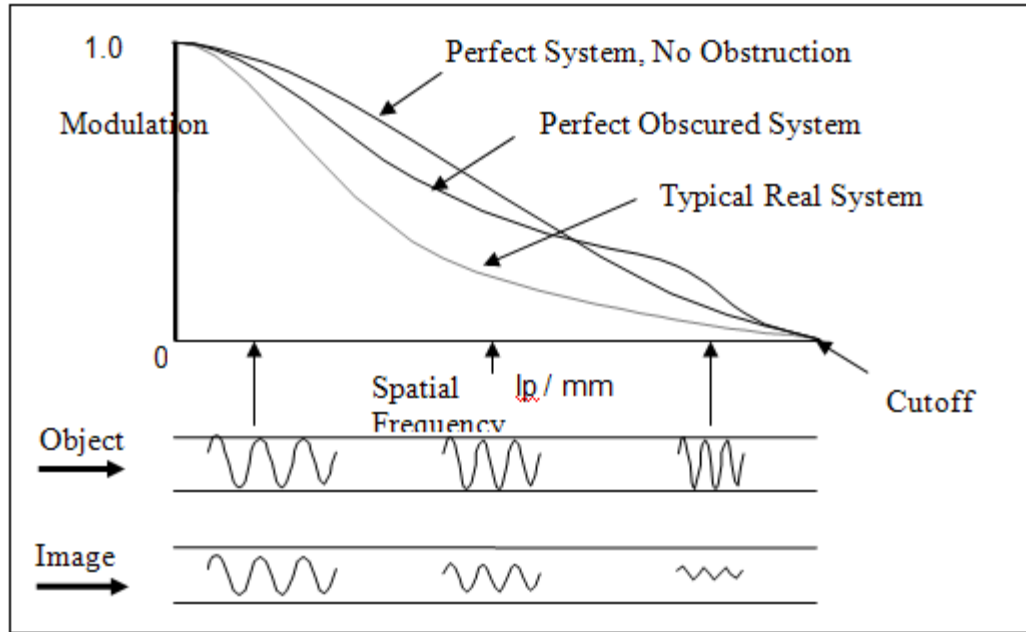


Figure 2-19.MTF vs. frequency

$$\text{Detector (Nyquist) Cutoff Freq : } \nu_0 = \frac{1}{\text{pixelpair}} \text{lp/mm} \quad (2.25)$$

- Vignetting

Vignetting is the reduction of an image's brightness at the corners compared to the image center. The reason for vignetting is that the rear elements are shaded by elements in front of them, which reduces the effective lens opening for off-axis incident light. The result is a gradual decrease in light intensity towards the image periphery [22].

## CHAPTER 3

### SYSTEM DESIGN

Imaging system composes of two main parts as optical part and detector part. At the very beginning of a system design, designer must clarify the system requirements. After that, according to these requirements, available materials for both detector and the optics can be determined. In addition to the detector material, designer should take into account the detector parameters during the design process. Moreover, flux on the detector is important to see that enough radiation is collected by the aperture of the system. So, signal to noise ratio can be calculated to see output signal. And finally, defining all these parameters, it is possible to start the design process.

#### 3.1 System Requirements

As stated before the SWIR range is in interest and the InGaAs detectors are used in this part of spectrum because they do not need to cool. and they can operate room temperature. In this thesis, general parameters for InGaAs detectors are used. 25  $\mu\text{m}$  is the minimum pixel size that can be used for SWIR spectrum. Therefore, while calculating the effective focal length for desired resolution, pixel size is taken as 25  $\mu\text{m}$ , as a constant parameter. Flux and signal to noise ratio are also calculated according to this parameters. Parameters of this detector are given in the Table 1.

Table 1. Detector parameters [23],[24],[25].

	unit	Min.	Value	Max.
Dark current	pA	0.2	0.4	1
Redout noise	electrons		800	
Saturation charge	Me.(electrons)		5	
Pixel size	$\mu\text{m}$	25	25	500
Readout rate	Mhz	0.01		2.5

### 3.1.1 Focal Length and f- number

The aim is to calculate the effective focal length of the system for  $\pm 5^\circ$  FOV(Field of view). Once the detector size and the FOV of the system are specified, the effective focal length of the optical system also gets fixed.

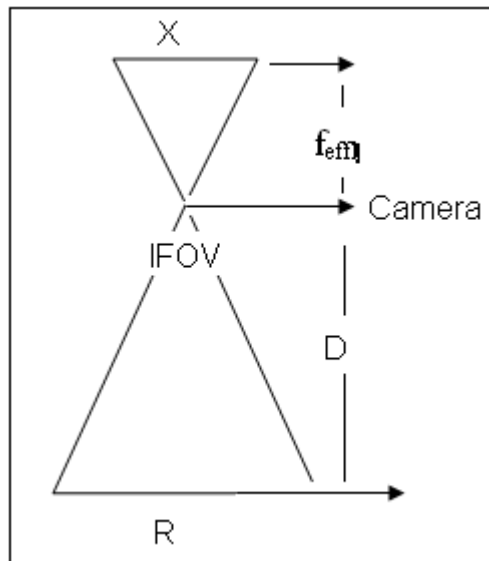


Figure 3-1 Relation between  $f_{eff}$ , resolution, pixel size and distance of the camera from ground.

Where,

D: Distance of the camera from ground

R: Resolution of the camera

X: Pixel size of the camera

IFOV: Instantaneous field of view

Using the triangular similarity Figure 3-1 is plotted and by using the Figure 3.1, Eq. 3.1 is written.

$$\frac{f_{\text{eff}}}{D} = \frac{X}{R} \quad (3.1)$$

then

$$f_{\text{eff}} = \frac{D * X}{R} \quad (3.2)$$

Using the Eq. 3.2,

$$f_{\text{eff}} = \frac{8 * 10^6 * 25 * 10^{-3}}{10^3}$$

Effective focal length is found to be 200 mm for this system.

Also by using Figure 3.1 IFOV can be found.

$$\text{IFOV} = \theta = 2 \arctan \frac{R/2}{D} \quad (3.3)$$

IFOV=25''

Using this value, and the Eq. 3.4

$$\text{FOV} = \text{IFOV} \times \# \text{ of pixels} \quad (3.4)$$

number of pixels calculated as 1.9 Mpixel.

Also image plane size was calculated from the equation;

$I = \# \text{ of pixels} * \text{pixel size}$  and then its size was calculated as 34.99mm. Also with same way swept area is found to be 1400m.

Another important parameter, the f-number can be found by using Eq. 3.5

$$f - \text{number} = \frac{f_{\text{eff}}}{\text{EPD}} \quad (3.5)$$

From the Eq. 3.5, f-number is calculated as 6,66.

Flux can be increased by increasing the integration time or increasing the f-number, since  $f_{\text{eff}}$  is fix; EPD can be decreased or increased to adjust it.

### 3.1.2 Flux Calculation

The sensor is sensitive to electromagnetic radiation incident upon its aperture. This radiant energy can come from any of the followings.

- Reflection from the object
- Emission from the object

In this study detector is sensitive to the reflected radiation. And the source of the reflected energy is the sun.

While calculating the signal to noise ratio, the total number of electrons, in other words, flux is used. The data for flux calculation are taken from ASTM G-173 Standards. SMARTS2 (Simple Model of the Atmospheric Radiative Transfer of Sunshine) is used for to generate the Data. In Figure 3-2 the reference spectra for flux data is shown. Also as seen in Figure 3-2, there is a considerable energy loss after passing through the atmosphere because of the absorption and the scattering especially at some regions transmission decreases to zero.

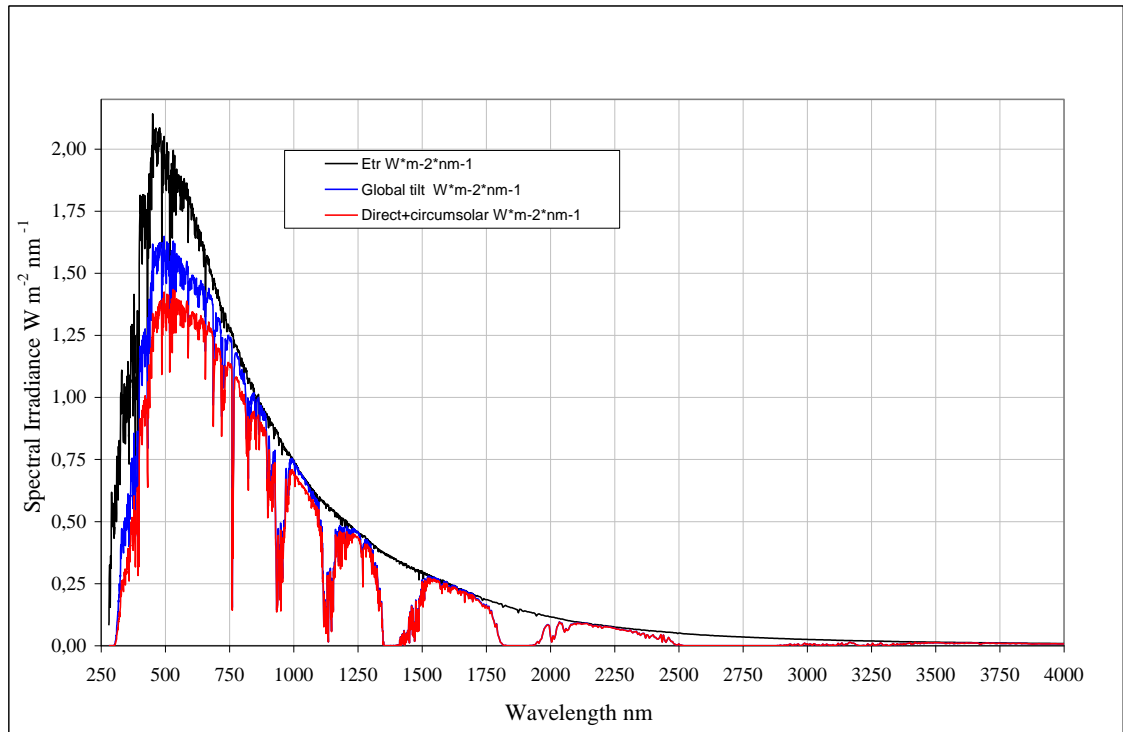


Figure 3-2. ASTM G-173-03 Reference spectra for solar irradiance [26]

Where,

ETR: Extraterrestrial Radiation (solar spectrum at top of atmosphere) at mean Earth-Sun distance.

Direct: The amount of solar radiation from the direction of the sun.

Circumsolar: Spectral irradiance within +/- 2.5 degree (5 degree diameter) field of view centered on the 0.5 deg diameter solar disk, but excluding the radiation from the disk

"Global Tilt": Total solar radiation; the sum of direct, diffuse, and ground-reflected radiation which is reflected from ground on south facing surface tilted 37° from horizontal

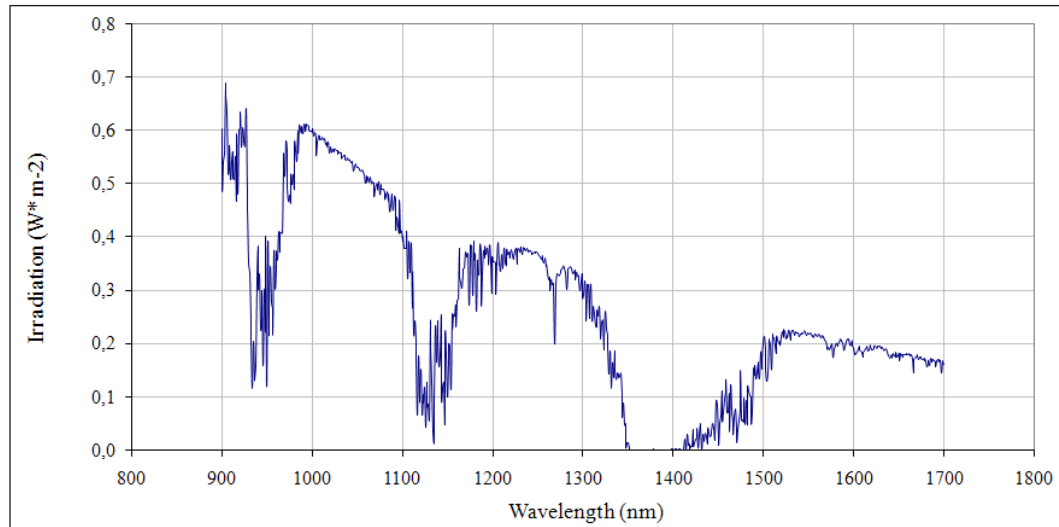


Figure 3-3. Wavelength vs. radiation before entering the ground ( $M_1$ )

$$M_1(\lambda) = ((M_{\text{global}}(\lambda) + M_{\text{direct}}(\lambda)) + (M_{\text{direct}}(\lambda) * \text{Cos}\theta)) \quad (3.6)$$

Where  $M_1$ : Irradiance on the ground.

Using the data from Figure 3-2 and Eq. 3.6, irradiance on the ground is calculated.

The data can be seen from Figure 3-3. Note that  $\theta$  is taken as  $37^\circ$ .

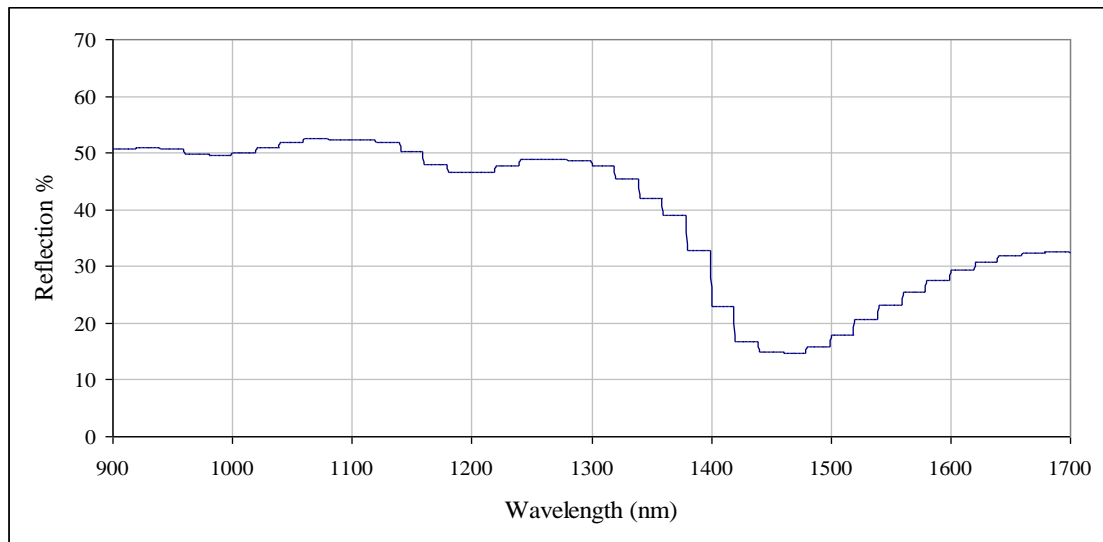


Figure 3-4. Wavelength vs. reflection coefficient for green grass [7]

In Figure 3-4, the relative reflection ratio can be seen for green grass. This ratio decreases to 15% at the 1450 nm. The maximum reflectivity is 53% at the 1100nm.

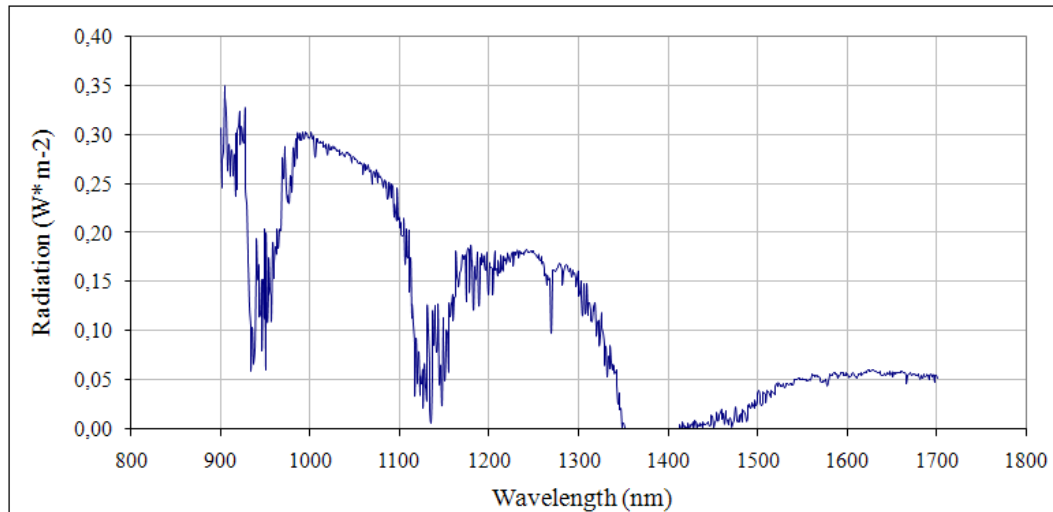


Figure 3-5. Wavelength vs. radiation after reflection from ground ( $M_2$ )

$$M_2(\lambda) = M_1(\lambda) * R(\lambda) \quad (3.7)$$

Where  $M_2$ : Irradiance reflecting from ground

When energy comes to the ground, it is reflected back, because of absorption of the material like soil, there also occurs some additional loss. As seen in Figure 3-5, energy is calculated after reflection from the green grass by using the Eq. 3.7.

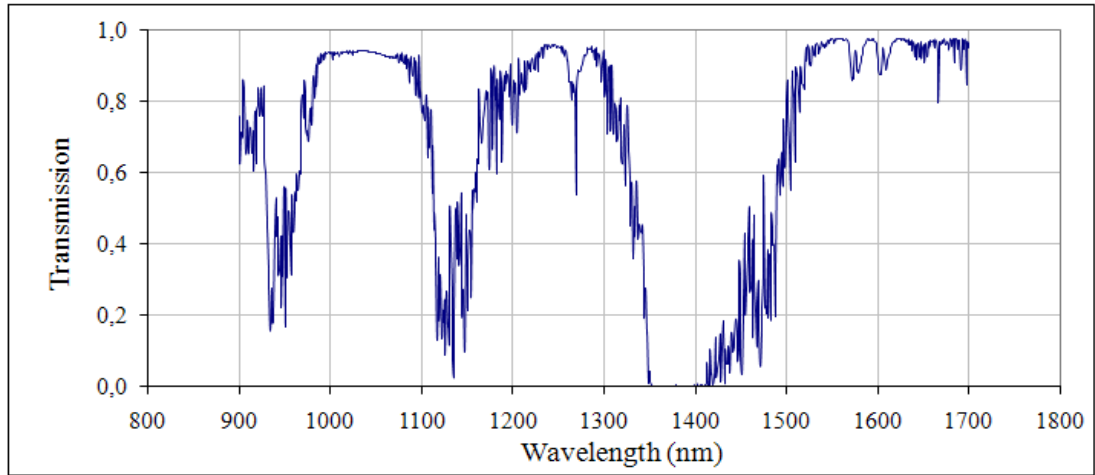


Figure 3-6. Transmission of atmosphere

$$T_{A1}(\lambda) = \frac{M_{\text{direct}}(\lambda)}{M_{\text{Ent}}(\lambda)} \quad (3.8)$$

Where  $T_{A1}$  : Atmospheric transmission

In Figure 3-6, transmission of the atmosphere is calculated from data at ASTM standards using the Eq. 3.8.

$T_{A2}$  is atmospheric transmission after reflection from ground until the radiation enters to optical system aperture. Transmission graph after reflection is shown in Figure 3-7. Transmission of the atmosphere data for 8 km is obtained using MODTRAN for 5 km visibility weather conditions.

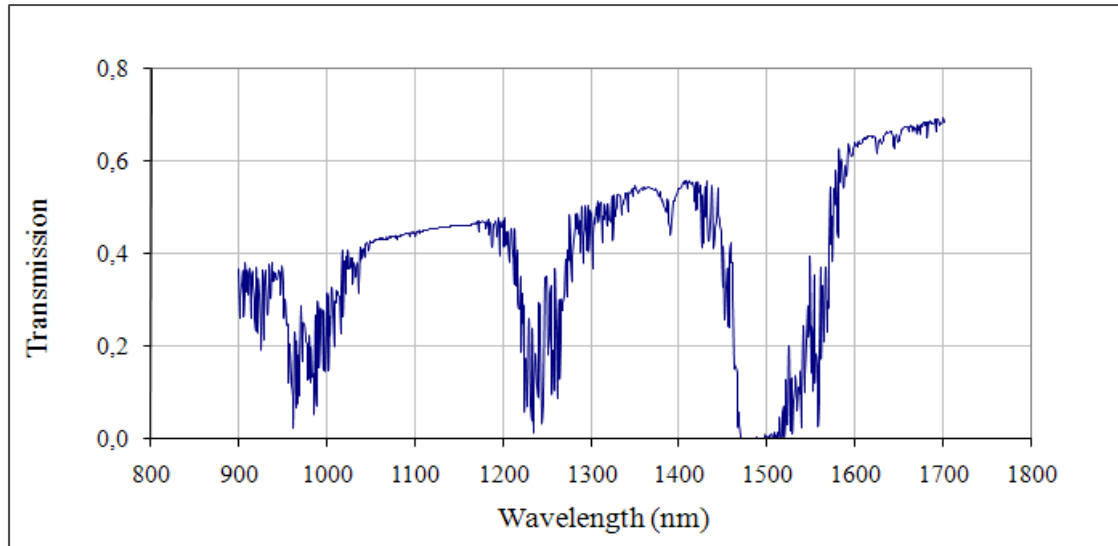


Figure 3-7. Atmospheric transmission for 8 km distance from the ground

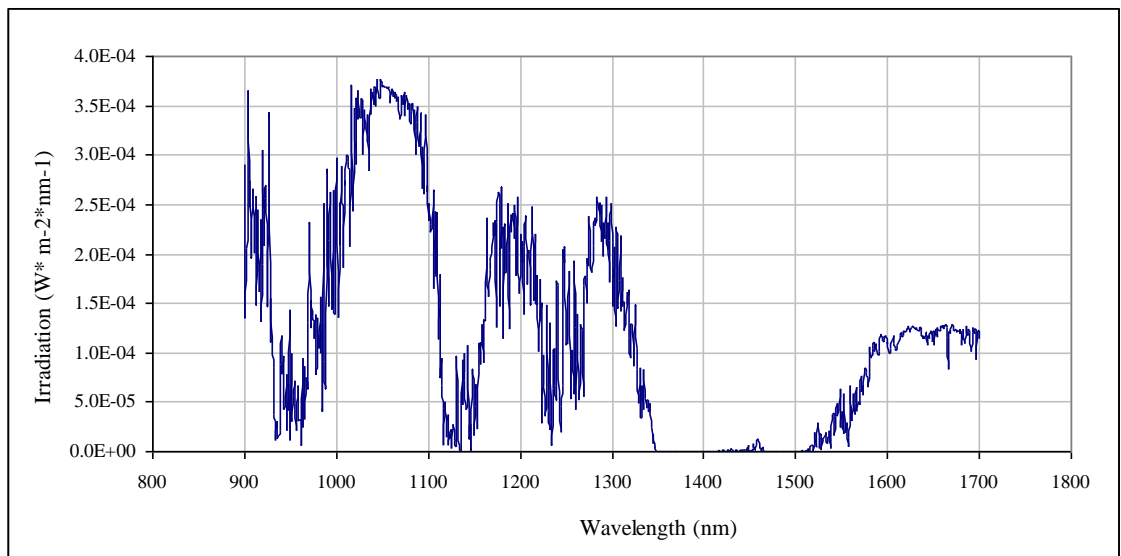


Figure 3-8. Wavelength vs. irradiation on the detector ( $M_D$ )

$$M_D(\lambda) = \frac{M_2(\lambda)}{4(f - \text{number})^2} * T_{A1}(\lambda) * T_{A2}(\lambda) * T_{\text{optics}}(\lambda) \quad (3.9)$$

Where,

$M_D$ : Irradiance on the detector

$T_{optics}$ : Transmission of optical system

Using the Eq. 3.9 total irradiance on the detector is found as 0,09 W .

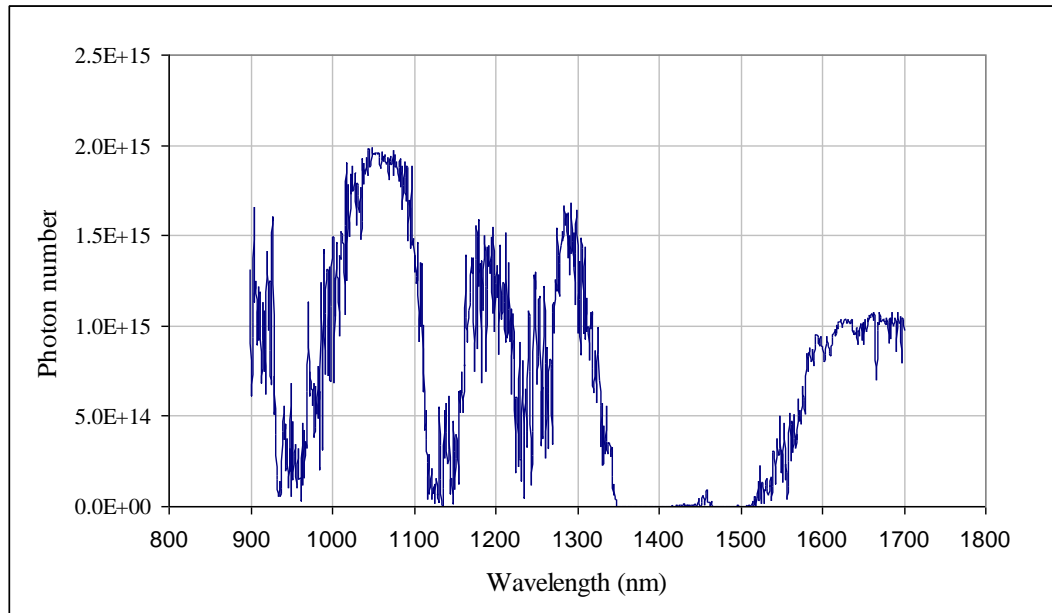


Figure 3-9 Wavelength vs. total photon number on the detector

$$n = \frac{E(\lambda)}{h\nu} \quad (3.10)$$

Using the Eq. 3.10 and data from Figure 3-8, number of photons were calculated (Figure 3-9). Using the quantum efficiency graph, total electron number is found to be  $4.48 \cdot 10^{+17}$  electrons/ second (Figure 3-10).

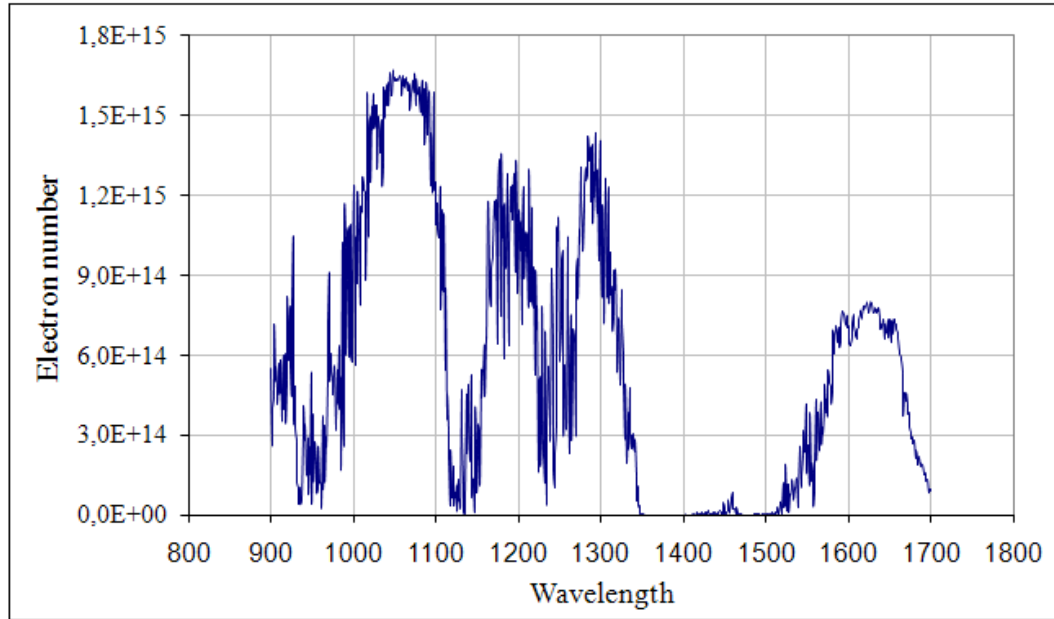


Figure 3-10. Wavelength vs. electrons on the detector.

For one pixel, number of electrons is found as  $2.2 \cdot 10^{+11}$  electrons/ pixel\*s is found.

### 3.1.3 Signal to Noise Ratio Calculation

A general way to express the reality of a detected signal and the precision of its measurement is to compare the signal  $S$  to the fluctuation of the background (i.e., the “noise” of the background). Traditionally, this is done by taking the ratio of the two quantities to form the “signal-to-noise ratio,” usually written as  $S/N$ ,

$$S/N = \frac{St}{\sqrt{(S + Bn_{\text{pix}} + I_d n_{\text{pix}})t + R_n^2 n_{\text{pix}} + \text{var}(B_t n_{\text{pix}} t)}} \quad (3.11)$$

Where;

- $S$  is the total number of photoelectrons received from the source per unit time

- $t$  (exposure time) is the integration time,
- $B$  is the number of photoelectrons received from the background (zodiacal light, atmospheric emission, and telescope thermal emission) per pixel and unit time,
- $I_d$  is the dark current of the detector expressed in electrons per pixel and unit time,
- $R_n$  is the readout noise per pixel (i.e., the standard deviation of the readout electrons collected per pixel for each read), and  $\text{var}(B_t n_{\text{pix}} t)$  is the variance of the estimate of the total background,  $B_t$  ( $B_t = B + I_d + R_n/t$ ), per pixel per unit time.

This last term reflects the uncertainty in the estimation of the background which does not arise from photon statistics; in other words, this term accounts for true variations [27].

While calculating the  $S/N$ , the noise ignored which are come from the tem  $B$ .

Also the  $S/N$  is calculated for the minimum and maximum time range for InGaAs detectors.

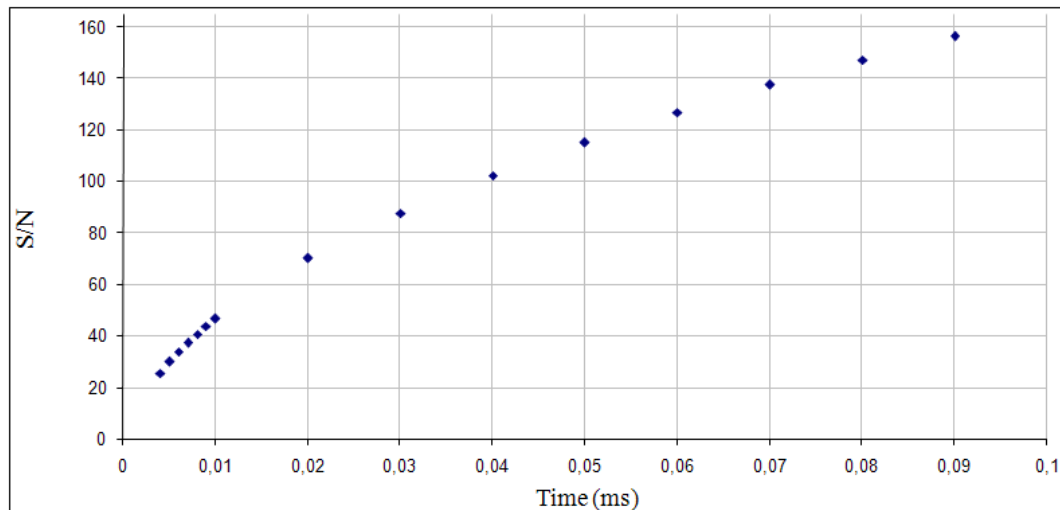


Figure 3-11. Integration time vs.  $S/N$

In Figure 3-11, it is seen that for minimum exposure time S/N is 25 and for maximum time, the value is 165. The calculated S/N range is quite sufficient for distinguish the signal from noise.

### 3.1.4 Rayleigh Resolution Criteria

Smallest desired resolution element should be matched in size to the minimum detector element [16] Resolution criteria (Rayleigh) for diffraction limited system is calculated as;

$$D = 1.22 \lambda \text{ f-number} \quad (3.12)$$

here D is the radius of the airy disk. Taking the resolution criteria into account, minimum resolution of the designed camera is calculated for  $\lambda = 0.9 \mu\text{m}$ . Rayleigh resolution is found as;

$$D = 7.3 \mu\text{m}$$

For other wavelengths relation between wavelength and the radius of the airy disk is plotted in Figure 3-12.

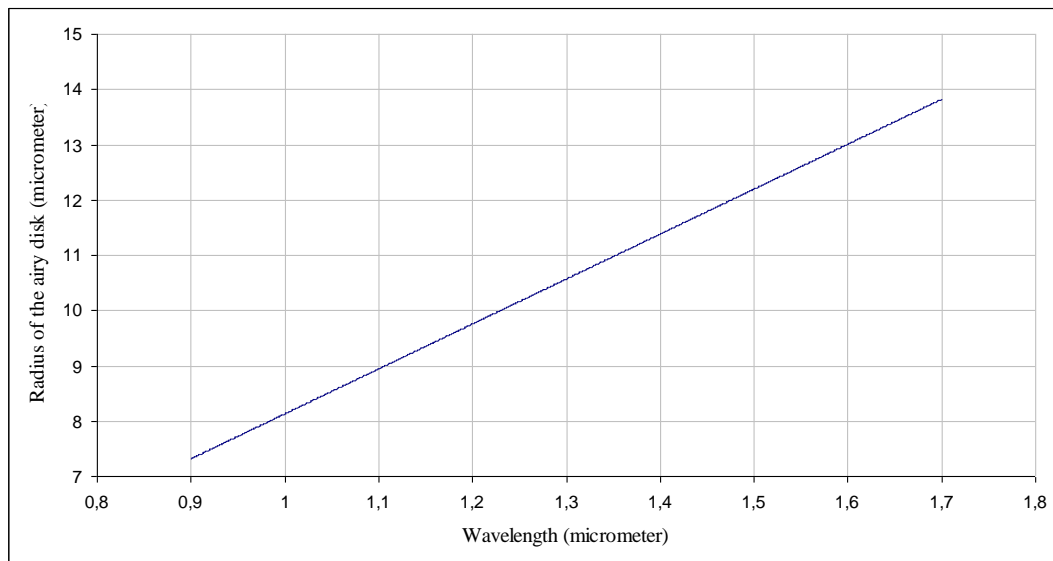


Figure 3-12. Radius of the airy disk vs. wavelength

A resolution criterion is necessary for matching the detector size with the airy disk radius, and for this design it is taken into account. If it is bigger than the detector pixel size, aperture of the system would be changed to adjust the airy disk since it is related to the f-number.

### 3.2 Optical Design

The process of ray focusing on the detector (focal surface) is provided by optical component of the camera. The design can be accomplished using one lens. However, the images are not good, crisp and uniformly bright across the whole field of view over a flat recording format [28]. In order to obtain high qualitative images, lens number can be increased, but then the transmission decrease which is important for detector illumination. While increasing the element number, there are some cases that should be in mind. Some of the improvement techniques are;

- Splitting
- Glass change
- Symmetry

Splitting the elements is into two or more approximately equal parts whose total power is kept same with the origin lens. This decreases the aberration since it allows the small incidence angle. Smaller angles introduce less aberration than large ones. In order to see the effect of splitting, at first, a design with single lens of which  $f_{\text{eff}}$  is 200 mm was done for the camera system on axis and monochromatic. The radius of curvatures for the lens' surfaces was found at the beginning of the design.

$$\Phi = \frac{1}{f} \quad (3.13)$$

From eqn. 3.13,  $\Phi = 0,005$  is found.

$$R_1 = \frac{2(n-1)}{\Phi} = -R_2 \quad (3.14)$$

For  $\lambda=1.7\mu\text{m}$ ,  $n=1.466$  (where  $n$  is taken for one of the glass which has high transmission value for SWIR.)

Radius of the curvatures are found to be  $R_1 = 186.4\text{mm} = -R_2$

Implementing these values on the design program with variables  $R_1, R_2$ , the system was optimized for  $f_{\text{eff}}$  and spherical aberration. Since the design is monochromatic and on-axis, there was only spherical aberration observed. After optimization spherical aberration was decreased to  $0.418 \lambda$  which was not sufficient for diffraction limited condition. It meant that minimizing the aberration using single lens was not possible. Bending the ray directly was not functioned, so splitting the power was done. To do this, the design was done with two lenses with the same glass and 1 mm air space in between them.

Radius of the curvatures are found to be  $R_1 = 372,8\text{mm} = -R_2 = R_3 = -R_4$

After optimization,  $0.418 \lambda$  was decreased to  $0.166 \lambda$  which was again much for design. Optimization was repeated with increasing the lens number to three, single glass and 1 mm air space between lenses.

Radius of the curvatures are found to be

$$R_1 = 561,44 = -R_2 = R_3 = -R_4 = R_5 = -R_6$$

Aberration was decreased to  $2.75 \cdot 10^{-6} \lambda$  which was very good for designer. But design parameters were not only on-axis and monochromatic. After decreasing the spherical aberration, other wavelengths were added the design. As a result, axial chromatic aberration is also arised. Best choice was to change the glass type for different lenses to minimize axial chromatic aberration. Achromatic doublets are examples for this work. In doublets one high index and one low index glasses are combined to decrease chromatic aberration. Lastly adding the off-axis rays, there arise distortion, field curvature, astigmatism, and coma. Splitting the lens is not enough for correct these aberrations. To decrease coma, distortion, lateral color aberrations symmetry principle is also used in symmetry principle one combine

the two opposite signed lenses then the aberrations caused by lens can be cancelled out by the other [29]. Also position of the stop is important for decreasing the off-axis aberrations. Thus sum of the aberrations is decreased at the focal plane and draft of the design is done in order to start optimization.

Table 2. System prescription data

Effective Focal Length	200	mm (in air)
Effective Focal Length	200	mm (in image space)
Back Focal Length	36.74	mm
Total Track	231.08	mm
Primary Wavelength	0.9	$\mu\text{m}$
Working F/#	6.6	
Image Space NA	0.07479476	
Object Space NA	1.5 10-009	
Stop Radius	14.486	mm
Paraxial Image Height	17.496	mm
Entrance Pupil Diameter	30	mm
Entrance Pupil Position	51.729	mm
Exit Pupil Diameter	17.137	mm
Exit Pupil Position	-114.223	mm
Maximum Radial Field	5	

The values of the aberrations are controlled by the merit function editor before and after optimization. The parameters like thickness, curvatures, and type of glasses of the lenses and the position of the lenses were simulated to correct aberrations of image at the focal surface. These simulations were repeated several times for the different fields (from center to the edge) and wavelengths. The prescription data is

given in the Table 2 for the system design. Also the specifications of lenses are given in the Table 3 which are used in the design. The index values are given for wavelength  $0.587\mu\text{m}$ .

Table 3 System lens parameters

	R1 (mm)	R2 (mm)	Thickness (mm)	Index (nd)	Material
Lens 1	97.723	51.122	4.3	1.623657	N-F <sub>2</sub>
Lens 2	72.729	805.821	9	1.475720	BaF <sub>2</sub>
Lens 3	110.179	-1018.206	7.5	1,393011	LIF
Lens 4	80.609	67.704	5	1,393011	LIF
Lens 5	-88.810	-59.849	5	1.475720	BaF <sub>2</sub>
Lens 6	-44.735	-85.423	5	1.623657	N-F <sub>2</sub>

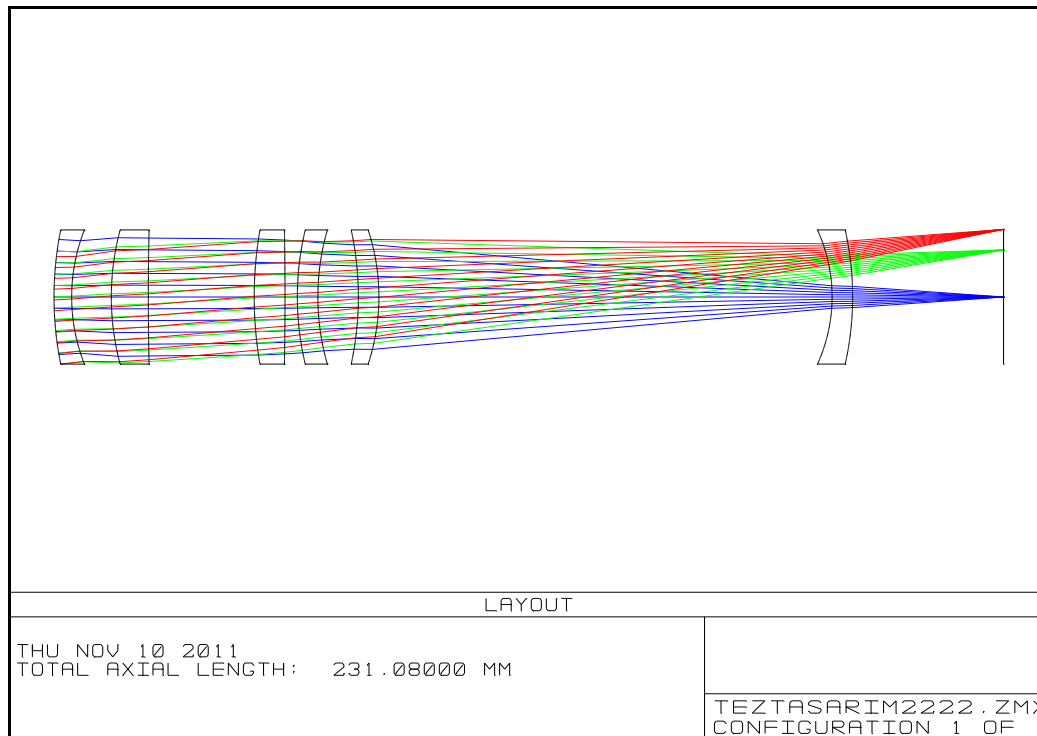


Figure 3-13. 2D layout of designed system

As seen in Figure 3-13, three fields were used, while looking at the image surface analysis. The first one is on-axis for zero fields, the second one is maximum field for off-axis and the third one is sub radius for off-axis field. The sub radius is found 0.7 from the unit circle. Using the sub radius, the third field is found  $3.5^\circ$ . The system is composed of six lenses, the second, third, and fifth lenses are convergent and the first, fourth, and sixth lenses are divergent (Table 3).

### 3.2.1 Glass Selection

There is not much choice for lens materials in the near infrared region. Chromatic aberration has been a problem in refractive optics especially when a wide wavelength is used. Oliva and Gennari studied that  $\text{BaF}_2$  and infrared glasses are the best combination to minimize chromatic aberration. After literature search,  $\text{BaF}_2$ ,  $\text{CaF}_2$ ,  $\text{ZnSe}$  and Fused Silica can be chosen as available lens materials because of their high transmission rate in the near-infrared wavelength and ease of fabrication. [30] [31] [32].

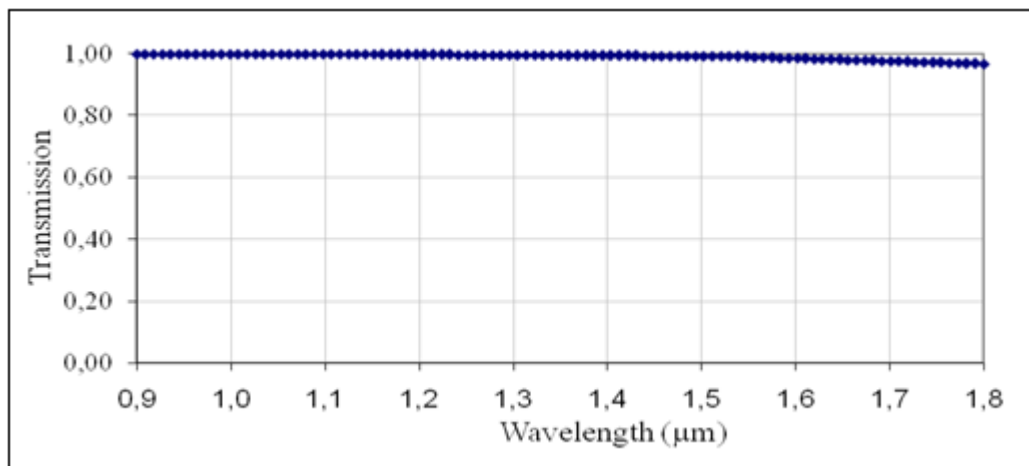


Figure 3-14. Internal transmission graph for the  $\text{N-F}_2$  lenses through 10 mm thickness

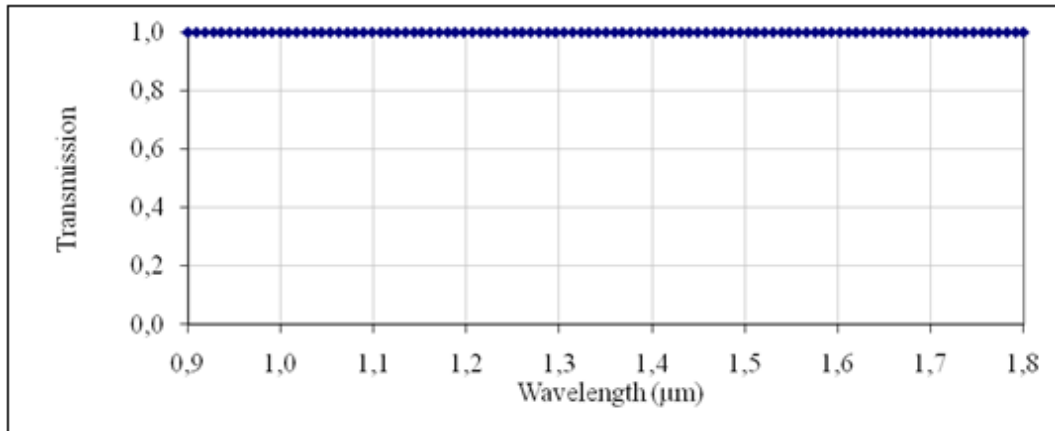


Figure 3-15. Internal transmission graph for the LiF lenses

So, during the selection of the glasses for the lenses was given priority to the transmission, availability and manufacturing. More than one glass was selected to decrease the chromatic aberrations. As seen in Figures 3-14, 3-15 and 3-16, transmissions are above the 0.95 for N-F<sub>2</sub>, LiF, BaF<sub>2</sub> lenses through the 10 mm, which is important for detecting the signal.

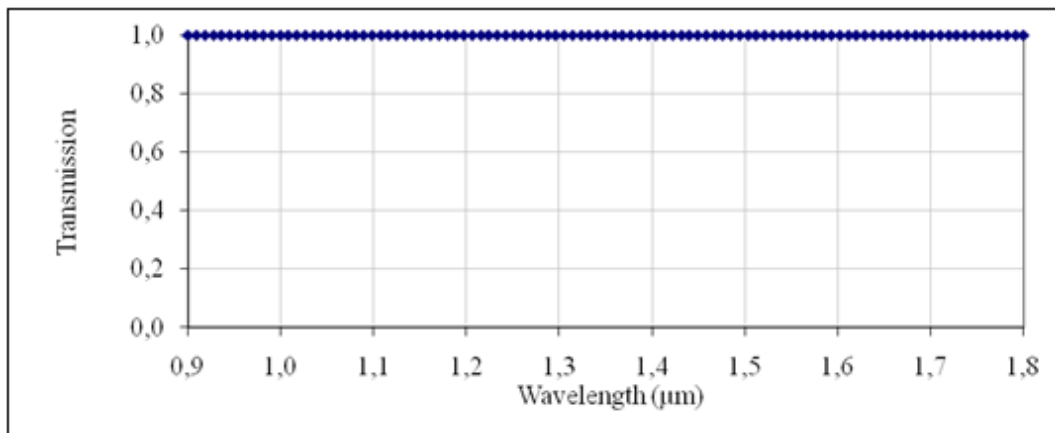


Figure 3-16. Internal transmission graph for the BaF<sub>2</sub> lenses

### 3.3 System Performance

As it was stated previously, the Rayleigh limit for image quality is wavefront aberration, OPD, varies no more than one quarter-wavelength over the aperture of an optical system. If it is provided, then image will be sensibly perfect. Afterwards the aim is obtain the diffraction limited performance for the designed system.

In order to evaluate the optical performance, (image quality, energy distribution) Aberrations, Spot diagrams, Distortion, Enclosed Energy, and MTF results are used.

#### 3.3.1 Seidel Aberrations

As seen in Table 4, values of the Seidel aberrations except distortion are lower than the  $\lambda/4$  which provides the diffraction limited condition. Figure 3-17 shows the third-order Seidel aberration coefficients as a histogram for each surface, and as a system sum. It helps to identify easily those surfaces that add or subtract most of a certain aberrations, and also which surfaces are balancing aberrations. For example much spherical aberration comes from second surface, third and tenth surfaces decrease this aberration up to  $\lambda/12$ . Also this situation is valid for other aberrations; if optical elements are combined with aberrations of opposite signs, then the result is that aberrations arise to the system by one lens canceled out by the others and then sum of the aberrations is decreased at the focal plane.

Table 4. Numerical values of Seidel aberrations (in  $\lambda$ ).

SPHA	COMA	ASTI	FCUR	DIST	CLA (CL)	CTR (CT)
$W_{040}$	$W_{131}$	$W_{222}$	$W_{220}$	$W_{311}$	$W_{020}$	$W_{111}$
0.08	0.07	0.09	0.23	-9.17	-0.04	0.07

One can also check the OPD analysis for the diffraction limited condition. As seen Figure 3-18, for all wavelengths and fields, wavefront errors are lower than the one quarter wavelength.

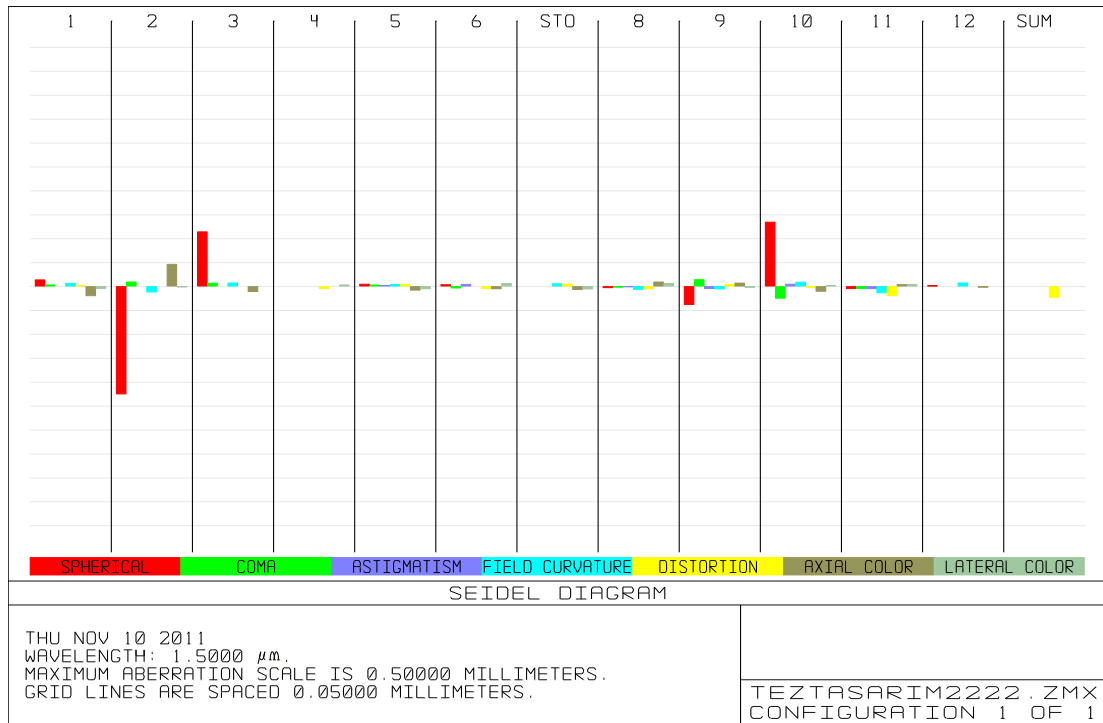


Figure 3-17. Primary aberrations for each surface and sum of them on the image plane

As seen in Figure 3-18, largest OPD occurs at the shortest wavelength at the edges. The shape of the curves also gives the idea about the aberrations through the aperture for the fields. For example; in the first field spherical aberration, in the second field astigmatism and in the third field chromatic aberrations are dominated. If aberration occurs much at the edges than at the center aperture can be adjusted by decreasing the aberrations.

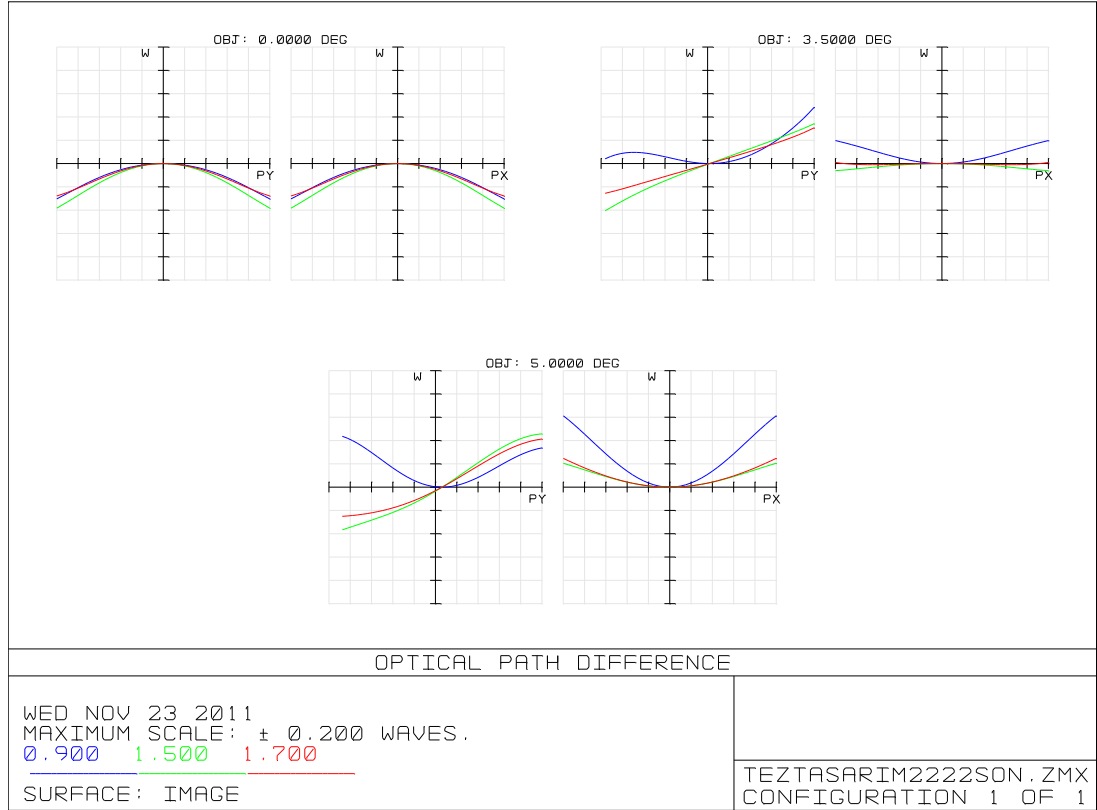


Figure 3-18. OPD fan plot for 3 fields

### 3.3.1.1 Distortion

The relative distortion is calculated using Eq. 3.14.

$$\text{Distortion} = 100 \times \frac{y_{\text{chief}} - y_{\text{ref}}}{y_{\text{ref}}} \quad (3.14)$$

As seen in Figure 3-19, positive (pincushion) distortion occurs in field three for primary wavelength at the edges. Its value is about 3. % and takes the maximum value at this field. For other fields this value is about 1 %, but these values do not affect the image, because human eye can resolve only 1% distortion. [18]. Distortion can be controlled by the computer codes, if it is much more than expected.

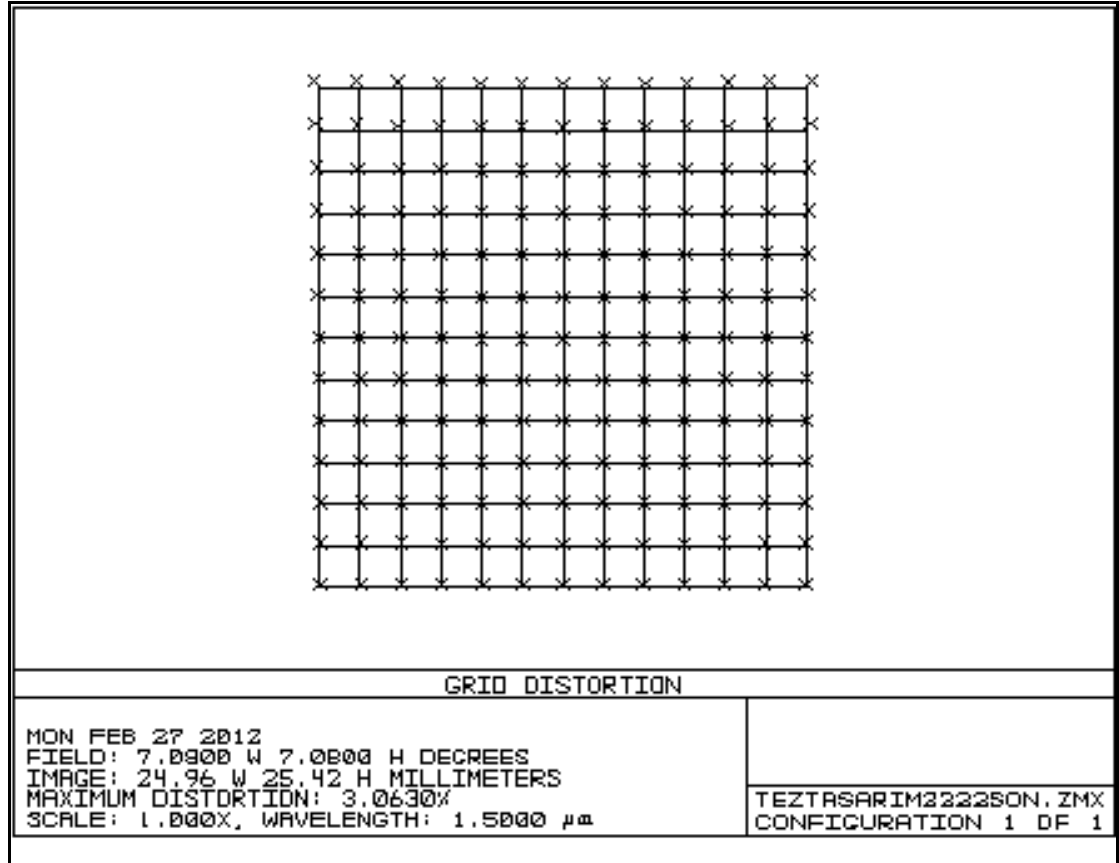


Figure 3-19. Grid distortion for 5 degree field

### 3.3.1.2 Field Curvature

In Figure 3-20 it is seen that the field curvature of the designed camera for main wavelength occurs at the maximum field. There is the longitudinal departure of the focal plane from ideal image surface and its maximum value 60  $\mu\text{m}$  at the edge of the optical axis. Spot size is evaluated for this shift to see the effects.

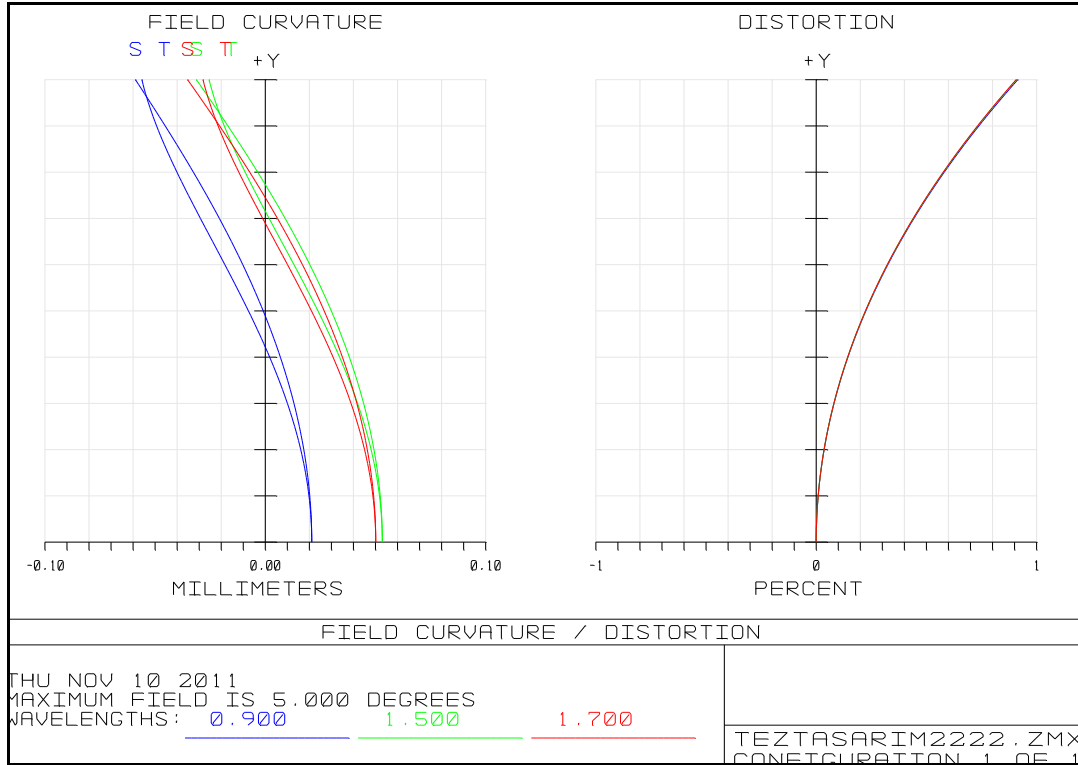


Figure 3-20 Field curvature

### 3.3.1.3 Lateral Color

Lateral color is the distance on the image surface from the intercept of the chief ray at each wavelength to the primary wavelength (0.9  $\mu\text{m}$ ) chief ray intercept. As seen in Figure 3-21, at the maximum field, this value is 1.6  $\mu\text{m}$  for second wavelength and has a negligible value.

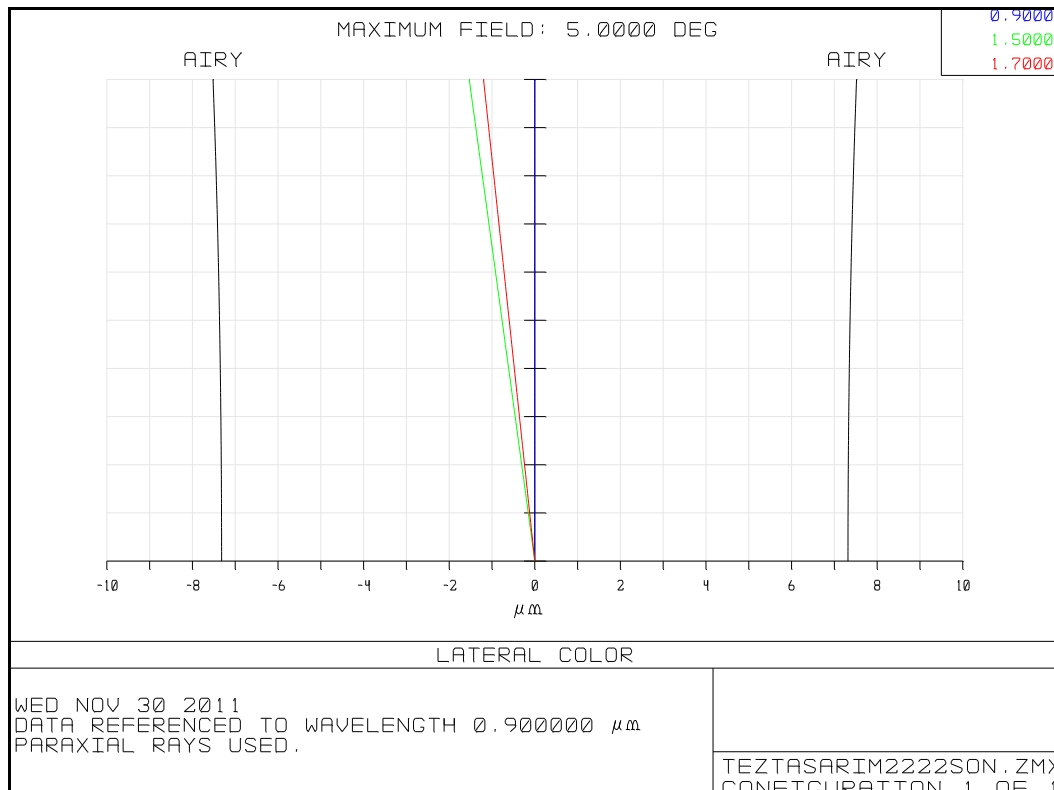


Figure 3-21. Lateral color

### 3.3.1.4 Chromatic Focal Shift

The diffraction limited depth of focus is calculated by the Eq. 3.15 by the Zemax.

$$\delta = \pm 4\lambda(f - \text{number})^2 \quad (3.15)$$

where  $\lambda$  is the primary wavelength.

Using the Eq. 3.15, diffraction limit for  $\lambda=0.9 \mu\text{m}$  is calculated as  $159.9 \mu\text{m}$ . However, as seen in Figure 3-22, in the designed system, the maximum chromatic focal shift is  $32 \mu\text{m}$  which is much lower than the diffraction limit.

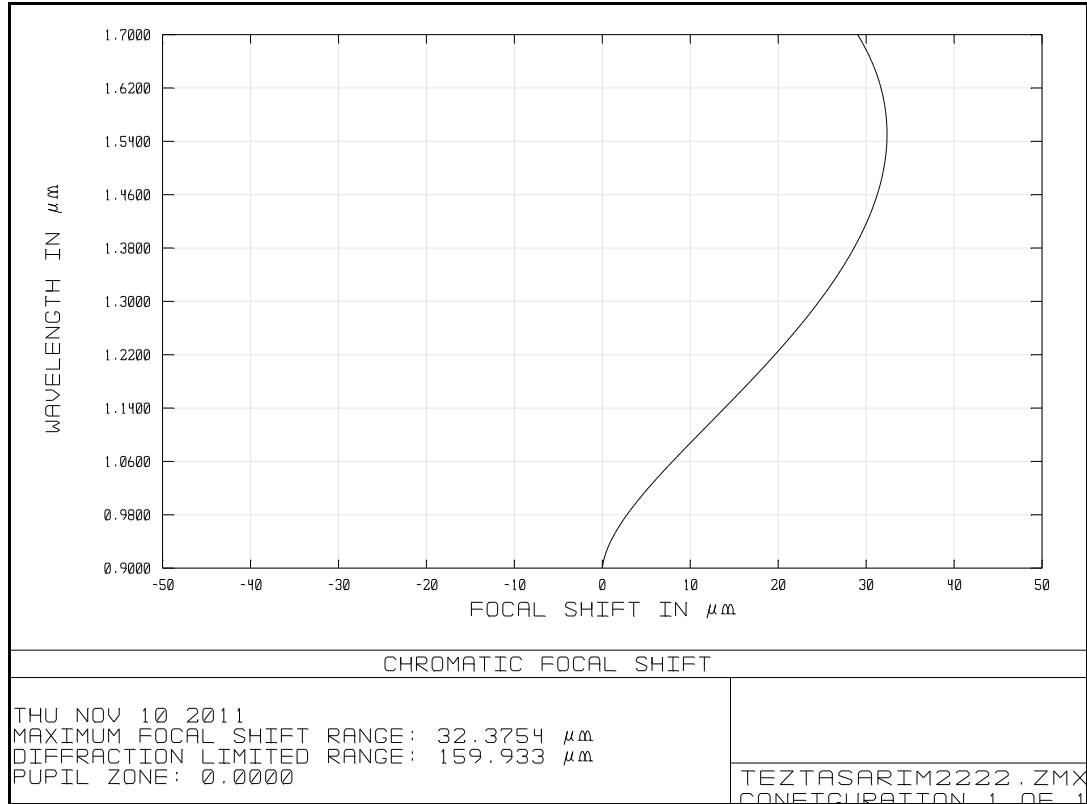


Figure 3-22. Choromatic focal shift

### 3.3.2 Spot Diagram

For diffraction limited systems, spot size should be in the airy disk.

From Eq. 2.22, airy disk radius is calculated as 7.32 μm where the wavelength is 0.9 μm and the f- number is as 6.66.

It can be seen in Figure 3-23, spot radius (geometric radius) varies from 2.24 μm to 2.89 when it goes from the center of the image (on-axis) to the edge of the field on the image plane. For good imaging, spot RMS radius should be smaller than the airy radius, because 68% of the energy is contained in the airy radius. RMS radius is taken into account while making the optimization.

Also spot diagram gives quick interpretation about the aberration. As seen in Figure 3-23, in the first field there is spherical aberration, in the second field there are coma and astigmatism and in the third field astigmatism in sagittal plane and chromatic aberration are dominated. But these aberrations do not affect much the image since spot radius is smaller than the airy disk for all fields.

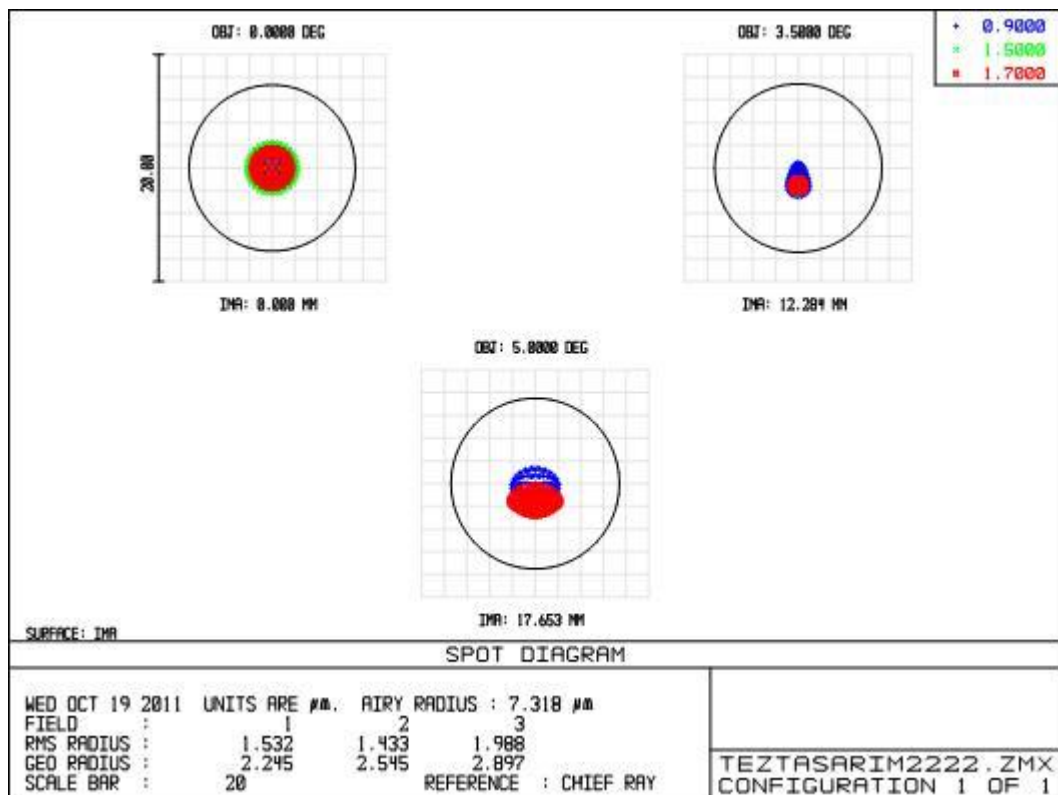


Figure 3-23. Spot diagram for different fields.

Focal plane shifted 30 μm in the range of chromatic focal shift, spot is also in the airy disk and image is not affected by this as seen in Figure 3-24. And also coma is more explicit for field two and astigmatism for field three in Figure 3-24 and Figure 3-25 than as Figure 3-23

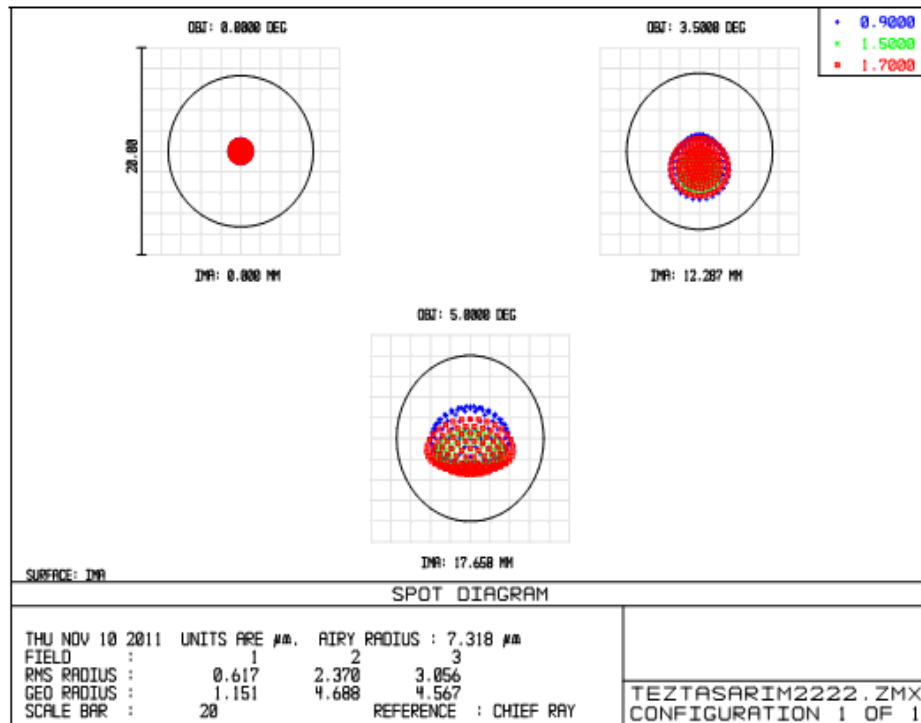


Figure 3-24. Spot diagram after shifting the focus 30  $\mu\text{m}$ .

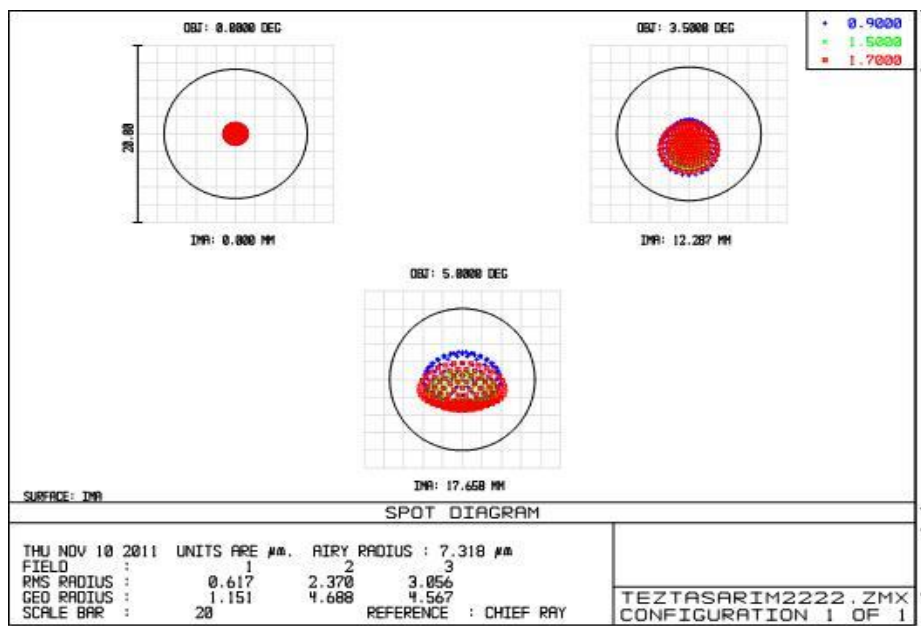


Figure 3-25. Spot diagram after shifting the focus 50  $\mu\text{m}$

Also focal plane shifted 50  $\mu\text{m}$  in the range of field curvature. In Figure 3-25, spot size is again in the airy disk and satisfies the diffraction limit condition.

### 3.3.3 Enclosed Energy

Enclosed energy is defined as the energy percentage plotted as a function of image diameter. For diffraction limited systems, 0.8 of the energy should be in the pixel size. In the designed system, 0.9 of energy is in the 25  $\mu\text{m}$  for all fields which is sufficient for the diffraction limited systems as it is indicated in Figure 3-26.

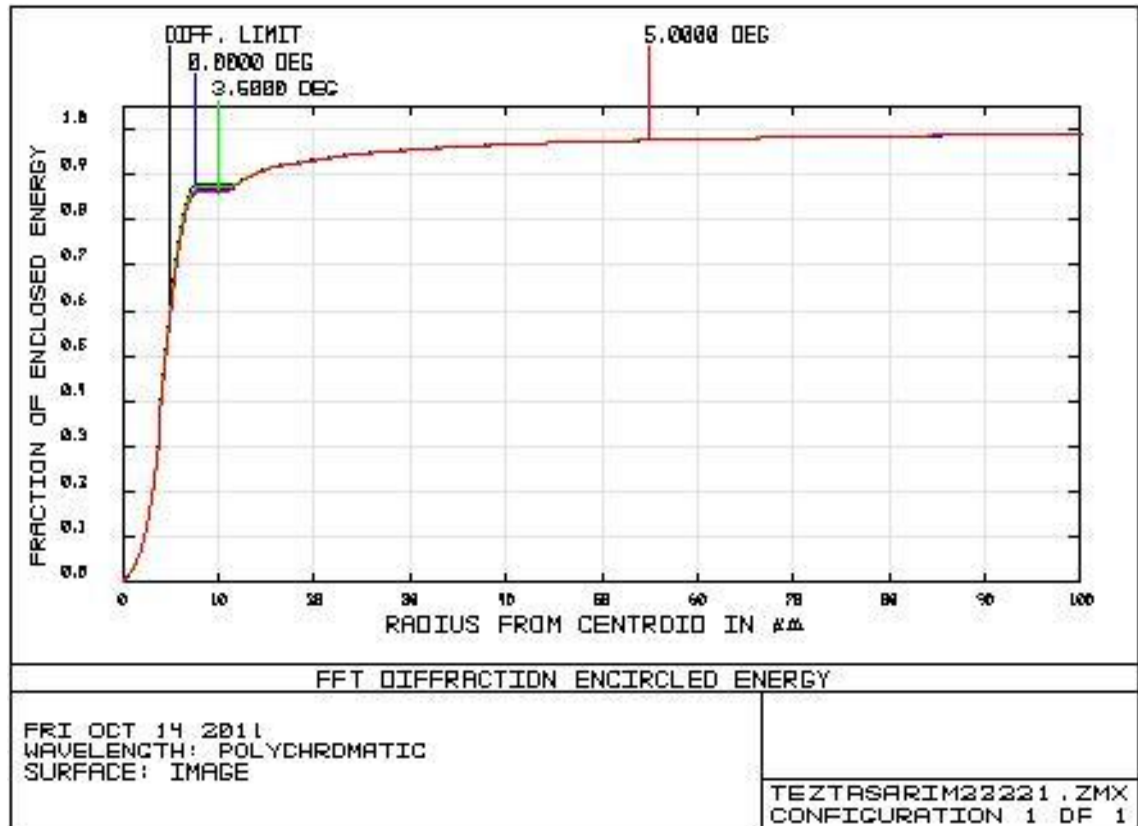


Figure 3-26. Fraction of enclosed energy.

### 3.3.4 MTF

As stated in Chapter 2, how well the modulation in an object is transferred to an image by the optics is defined by MTF and Nyquist frequency gives idea while interpreting the graph.

Using Eq. 2.23

$$\text{Detector Cutoff frequency} = \frac{1}{50 * 10^{-3}} \text{ lp / mm}$$

Detector cutoff frequency is found 20lp/mm.

Perfect contrast occurs for 100 % ratio. But at diffraction limited plot, it is perfect system, no obstruction. As seen in Figure 3-27, a Nyquist frequency value's contrast ratio is about 0.7 and very close to diffraction limit, which gives the good image.

MTF also gives idea about the aberrations but defining them is more difficult than OPD or Spot diagram etc.

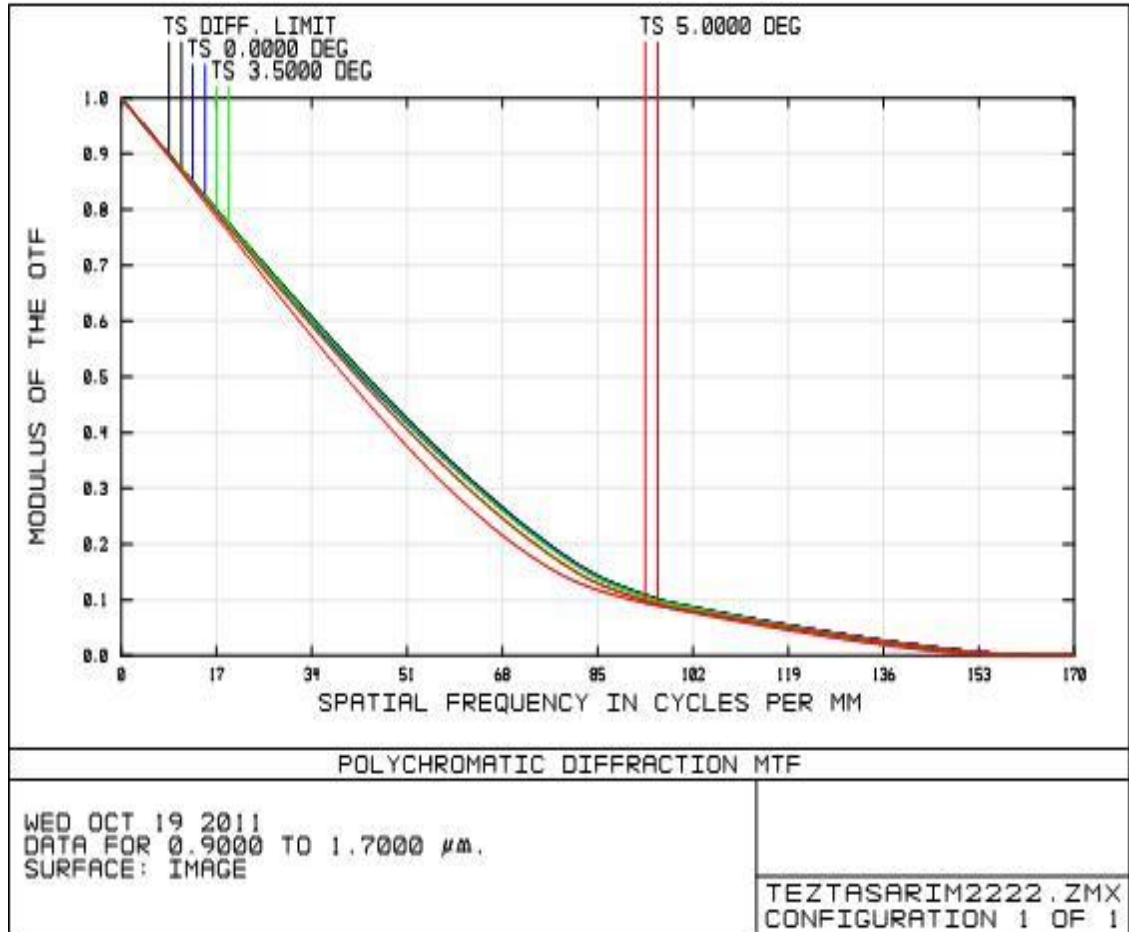


Figure 3-27. MTF

### 3.3.5 Vignetting

In order to decrease the vignetting value, semi diameters of the lenses were increased from 15.0mm to 17.5mm. This increases the transmission of the system. As seen in Figure 3-28 and 3-29, fraction of the unvignetted rays was increased from 0.80 to 0.95 at the edges. In Table 5, transmission ratio was given for all fields and wavelengths.

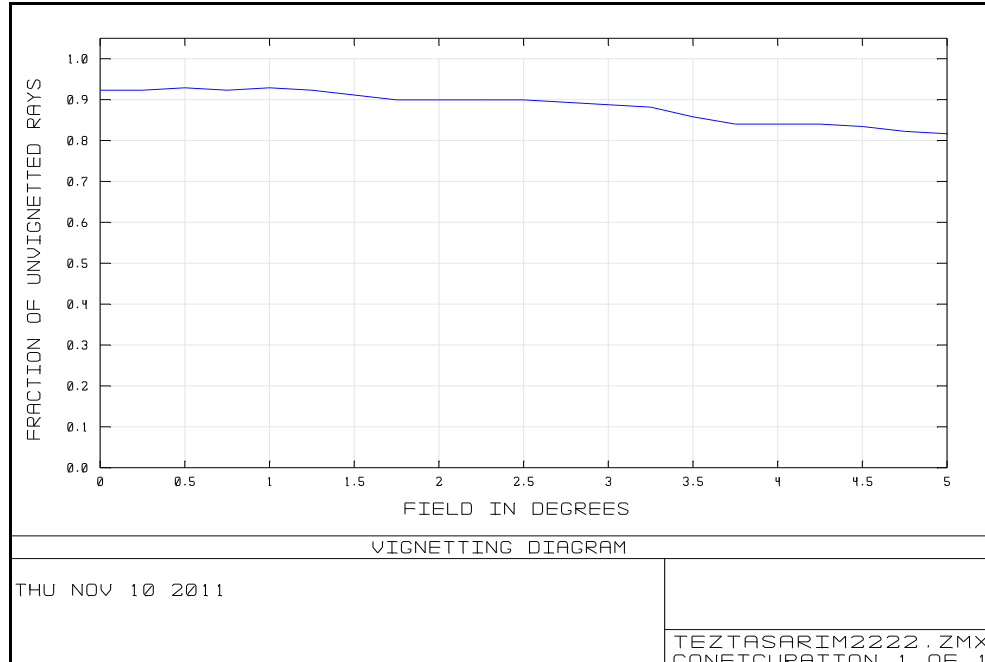


Figure 3-28. Vignetting diagram

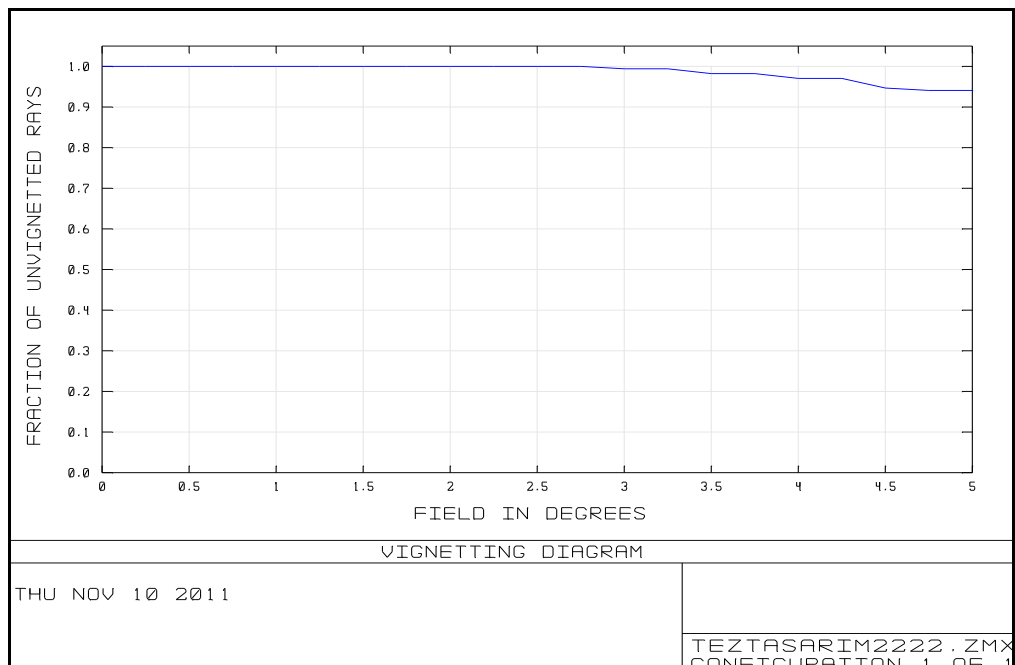


Figure 3-29. Vignetting diagram after optimization.

Table 5. Numerical values of transmission

Field Position	Wavelength (micron)	Transmission without vignetting %	Transmission with vignetting %
0.0 deg	0.9	61.96	61.96
0.0 deg	1.5	62.19	62.19
0.0 deg	1.7	61.39	61.39
3.5 deg	0.9	61.57	57.55
3.5 deg	1.5	61.78	57.75
3.5 deg	1.7	60.95	56.98
5.0 deg	0.9	58.61	54.62
5.0 deg	1.5	58.80	54.80
5.0 deg	1.7	57.98	54.03

## CHAPTER 4

### DISCUSSION AND CONCLUSION

In this study, the camera operating in the SWIR range was designed. Firstly, the atmospheric effects has presented for the flux calculation. Since the SWIR is a new approach for imaging, there are not much detector types other than InGaAs detectors. Therefore, it is constrained to use this detector in this work and 25 microns as a pixel size in the resolution calculations. Since space is limited with 50x50x300 mm for installation and object distance is defined as 8 km and resolution is defined 1 m from that distance, and also minimum pixel size is 25  $\mu\text{m}$ , focal plane is limited to obtain necessary resolution. And then, focal plane was calculated for the design and found as 200 mm, and total ray trace is 231.08 mm so there is also space for electronics.

Aperture affects the some of the aberrations like spherical, distortion etc., for that reason it is tried to decrease for minimizing them and fixed at the 30 mm. Then f-number is calculated as 6.66 which is important for the irradiance of the system.

After calculating the flux on the detector, the number of electrons was calculated for each pixel for one second. Using this information for minimum and maximum time range for detector, S/N is calculated and plotted. While doing this calculation, saturation of the pixel is taken into account. Thus, time range is defined for designed system which gives the sufficient energy to take the image.

While doing the design, the merit function editor is used to optimize, the parameters like radius, thickness, glass type, position and spacing between lenses and simulated to achieve high quality images at the focal surface. These simulations were done for three different field angles.

To obtain diffraction limited system, three different types of glass and six lenses are used with a total mass of 117.48 g. and also system is a refractive system configuration.

Because of chromatic wavelength and  $10^\circ$  FOV, aberrations are the problem. The primary aberrations like spherical aberration, field curvature, chromatic aberrations (lateral and longitudinal), astigmatism, coma and distortion are plotted and their values are evaluated. The aberration values are found in diffraction limit except for the distortion. Distortion was a bit much more than %1 but it can be corrected with computer program. OPD fan plot is plotted for see the aberrations through the aperture for all fields. Seidel histogram is plotted to see the aberrations for each surface and as a sum of them. Spot diagram is plotted to see the RMS spot diameter and RMS spot diameter is smaller than the airy disk diameter then all rays are in the airy disk. Performance tests were done and plotted to understand how well the image for the designed system is. To do so modulation transfer function (MTF), is plotted and Nyquist frequency is calculated as 20 lp/mm for this value, the modulation is higher than the %50 then it is enough for the contrast. Encircled energy is plotted to see energy ratio for the detector pixel size. It is seen that %80 of the energy is contained that within the diameter of 25  $\mu\text{m}$  which is a well match to the pixel pitch. Vignetting is plotted to see the loss rays from the edges and increased the lens diameters to prevent them. Finally, image simulation is done to examine and evaluate the system with detector.

Table 6. Parameters of the lenses and result of analysis after test plate optimization

		Value	Unit
Lens 1	R1	101.206	mm
	R2	52.222	
Lens 2	R1	72.161	mm
	R2	739.775	
Lens 3	R1	83.972	mm
	R2	3440.938	
Lens 4	R1	74.905	mm
	R2	57.945	
Lens 5	R1	-98.019	mm
	R2	-63.627	
Lens 6	R1	-45.136	mm
	R2	-85.877	
RMS spot diagram	Field 1	8.69	$\mu\text{m}$
	Field 2	4.02	
	Field 3	2.39	
Encircled energy @ 14 $\mu\text{m}$ radius		% 78	
MTF @ 20 lp/mm		%60	
OPD	Field 1	>0.4	$\lambda$
	Field 2	>0.2	
	Field 3	>0.2	

Thus this system is appropriate to the Rayleigh criteria and an image is sensibly perfect. This system can take good image of 1m resolution from 8 km distance. However, producibility is also important for the lenses that are used in the design. Reference test plates are used in order to confirm whether the intended surface quality is achieved or not in lens manufacturing. Due to this reason, designing the lenses that are appropriate with available test plates in stock decreases the cost and

time. The system design performed during this study was finally re-optimized using Zemax test plate fitting tool. At the end of this study, radiuses of the lenses were changed considering the available test plates and hence there have been changes in the analyses of the design performed with these radiuses.

The result of the analyses and radius of the lenses are given in Table 6. As seen from Table 6, RMS spot diagram radius is getting larger than airy disk for only field 1 and that value is not much and just affects the blur diameter of the image point on the detector. Also encircled energy decreased from %85 to % 78 and affects the energy distribution of the image on the detector. Since this value is again above % 70 percent, encircled energy was not influenced by optimization. MTF value is also above % 50 and sufficient for the related resolution for the point image. And finally OPD is also lower than  $\lambda/4$  for the second and the third fields.

To sum up, after making the test plate fitting optimization, the design is not as good as the first design theoretically; however taking the cost and time conditions into consideration, second design is more sensible for manufacturing.

## REFERENCES

1. North American AstroPhysical Observatory (NAAPO)  
<http://www.bigear.org/CSMO/HTML/CS13/cs13p24.htm>  
Retrieved on 10 November 2011
2. Zissis G. J., 1993, *The IR-EO Systems Handbook - Volume 1 - Sources of Radiation*, SPIE optical engineering press
3. Davers G. D., Turner D., 2008, Photonic Spectra InGaAs SWIR imagers get a better look when the heat is on.
4. Dawes G. D., 2010, The Key to Information-Rich Imaging, *Unmanned Systems* 30-32
5. Battaglia J, Brubaker R, Ettenberg M, Malchow D, 2007 High speed Short Wave Infrared (SWIR) imaging and range gating Cameras, *SPIE Vol. 6541* 654106-1
6. Gangopadhyay P. K., Meer F., Dijk P., (2008) Atmospheric modelling using FASCOD to identify CO<sub>2</sub> absorption bands and their suitability analysis in variable concentrations for remote sensing applications *Journal of Quantitative Spectroscopy & Radiative Transfer* 109 670–683
7. Smith F. G., 1993, *The IR-EO Systems Handbook - Volume 2 - Atmospheric Propagation of Radiation* SPIE optical engineering press

8. Xingcai Li a,b, LiXie a, XiaojingZheng (2012) The comparison between the Mie theory and the Rayleigh approximation to calculate the EM scattering by partially charged sand *Journal of Quantitative Spectroscopy & Radiative Transfer* 113 251–258
9. Alberta P., Smithb K.M., Bennartzc R., Fischera J., Newnhamb D., A2004, Satellite- and ground-based observations of atmospheric water vapor absorption in the 940 nm region, *Journal of Quantitative Spectroscopy & Radiative Transfer* 84 181–193
10. Cooper A. W. and Crittenden E.C., Jr. 1998, *Electro-Optic Sensors and Systems*, Naval Postgraduate School, Monterey, CA,
11. GOODRICH, <http://www.sensorsinc.com/whyswir.html>  
Retrieved on 13 December 2011
12. MODTRAN Ontar Corporation, 2005, *PcModWin Manual Version 4.0 v3r1 Version 1.2*, 9 Village Way, North Andover, MA 01845, USA.
13. Driggers, R G., Cox, P. and Edwards, T, 1993, *Introduction to Infrared and Electro Optical Systems*, Artech House, Inc. MA,
14. Smith G.H., 1998, *Practical Computer-Aided Lens Design*, Willmann-bell, Inc.,
15. Pedrotti, Frank L. and Pedrotti, Leno S., 1996, *Introduction To Optics*, Prentice-Hall PTR

16. Malacara D. D, Malacara Z., 2004, *Handbook of Optical Design*, MARCELUS EKKERIN, C.
17. Fischer, R. E., 1993, *Optical Design: Principles of Optical Systems Layout*, SPIE, The International Society for Optical Engineering
18. Warren, J. Smith, 2000, *Modern Optical Engineering*, McGraw-Hill
19. ZEMAX *Optical Design Program User's Guide Version 10.0*, Focus Software,
20. Dudzik M. C., 1993, *The IR-EO Systems Handbook - Volume 4 - EO Systems Design, Analysis, and Testing* SPIE optical engineering press
21. Holst, Gerald C., 1995, *Electro Optical Imaging System performance*, JCD Publishing, FL
22. WIKIPEDIA <http://en.wikipedia.org/wiki/Vignetting>  
Retrieved on 04 December
23. Bay Spec, <http://www.bayspec.com/userfiles/file/BaySpec-Datasheet%20-%20NCAM-0900-1700%20Near%20Infrared%20Camera.pdf>  
Retrieved on 28 December
24. Driesa C., Ettenberga M. H, Huang W., Masauna N., Langea M. and Onata B. M., 2007, Ultra Low Dark Current InGaAs Technology for Focal Plane Arrays for Low-Light Level Visible-Shortwave Infrared Imaging, *Infrared Technology and Applications SPIE Vol. 6542*

25. GOODRICH, <http://www.sensorsinc.com/arrays.html>  
Retrieved on 17 November 2011
26. ASTM International Standards <http://www.astm.org/Standards/G173.htm>  
14 August 2011
27. Pierre Y. Belly, 2002, *The Design and Construction of Large Optical Telescopes*, Springer
28. Joseph M. Geary, 2002, *Lens Design*, Willmann-bell, Inc.
29. Warren J. Smith, 1992, *Modern Lens Design*, McGraw-Hill
30. Optical design of MOIRCS Ryuji Suzukia,b, Chihiro Tokokua,b, Takashi Ichikawaa and Tetsuo Nishimurab aAstronomical Institute, Tohoku University, Sendai, Miyagi 980-8578, Japan bSubaru Telescope, National Astronomical Observatory of Japan, 650 North A'ohoku Place, Hilo, Hawaii 96720, USA
31. Janos Technology, [www.janostech.com](http://www.janostech.com)  
Retrieved on 03 January 2012
32. Ryder L. A., Jamieson T., 2005, Lens Design for the Near Infrared Camera for the James Webb Space. -*The International Society for Optical Engineering SPIE 5904-590409*